Available online at www.sciencedirect.com
ScienceDirect
Radiation Measurements 41 (2007) S78–S99
Radiation Measurements
www.elsevier.com/locate/radmeas

Optically stimulated luminescence and its use in medical dosimetry

M.S. Akselrod[a,*], L. Bøtter-Jensen[b], S.W.S. McKeever[c]

[a]*Landauer Crystal Growth Division, 723 1/2 East Street, Stillwater, OK 74074, USA*
[b]*Risø National Laboratory, Radiation Research Department, DK-4000 Roskilde, Denmark*
[c]*Department of Physics, Oklahoma State University, Stillwater, OK 74078, USA*

Abstract

The optically stimulated luminescence (OSL) technique has already became a successful tool in personal radiation dosimetry, geological and archeological dating, and in radiation diagnostic imaging. This review briefly describes the history of OSL. Significant advances have been made recently in the theoretical study of OSL to explain the behavior of radiation sensitive materials with several types of dosimetry traps, recombination centers and competing deep traps. Progress in material and detector engineering has allowed new and promising developments regarding OSL applications in the medical field. Special attention is dedicated to Al_2O_3:C as a material of choice for many dosimetric applications; present technology can provide Al_2O_3:C fiber sensors with diameters as small as 300 μm. A new RL/OSL fiberoptic system has a high potential for *in vivo* and *in vitro* dosimetry in both radiation therapy and diagnostic mammography. Different aspects of instrumentation, data processing algorithms, post-irradiation and real-time measurements are described.
© 2007 Elsevier Ltd. All rights reserved.

1. Introduction

Optically stimulated luminescence (OSL) is one of the many known stimulated phenomena in condensed matter that can be induced by ionizing radiation and that became a successful practical tool in radiation dosimetry. Until recently thermoluminescence (TL) dosimetry (TLD) was the most popular dosimetric technique when relatively inexpensive passive integrating detectors based on crystalline and glass materials (like LiF:Mg,Ti, CaF:Mn, $CaSO_4$:Dy, $Li_2B_4O_7$, alumophosphate glasses and others) were used (McKeever et al., 1995). Point defects in TL materials created during crystal growth or solid state sintering are able to trap electrons and holes generated during irradiation and this way can store dosimetric information for a long time. To measure an accumulated dose a TL detector is heated in a reader and emits luminescent light the amount of which is proportional to the absorbed dose. TLD is used for personnel radiation monitoring and medical dose verification. It is a destructive technique, in that the signal is completely removed from the detector since readout requires heating of a detector. Furthermore, it is slow and is not suitable for high spatial resolution imaging.

OSL utilizes materials and electronic processes similar to TL but interrogation of the detector is performed by light instead of heat (see Bøtter-Jensen et al., 2003). High sensitivity, precise delivery of light, fast readout times, simpler readers and easier automation are the main advantages of OSL in comparison with TLD. OSL allows for re-reads of the detector multiple times while maintaining the precision, and yet it is still can be used as an erasable measurement technique. In comparison with TL materials OSL phosphors are not subjected to heating at high temperature, do not experience the so-called "thermal quenching effect", and they can be mixed with or imbedded in plastic. The ability to make a composite detector is a significant simplification in detector manufacturing processes and allows one to mass-produce OSL detectors and imaging plates with tight tolerances in uniformity and sensitivity. Another major advantage of OSL over TL is its imaging capability. High-resolution imaging of radiation fields using OSL (sometimes termed as "photostimulated luminescence" (PSL)) is already a successful tool in personal dosimetry, in computer radiography (CR) and diagnostic imaging. OSL has also a strong potential for precise measurements in the radiotherapy dose range between 0.1 and 200 Gy.

OSL was first suggested as a dosimetry tool in the 1950s and 1960s (Antonov-Romanovskii et al., 1956; Bräunlich et al., 1967; Sanborn and Beard, 1967). The main obstacles for

* Corresponding author.
E-mail address: makselrod@landauerinc.com (M.S. Akselrod).

1350-4487/$ - see front matter © 2007 Elsevier Ltd. All rights reserved.
doi:10.1016/j.radmeas.2007.01.004

OSL application found at that time were: strong fading in case of relatively narrow band-gap sulfide materials like MgS, CaS and SrS doped with rare earth ions like Sm and Eu. Cu^{+}-doped fused quartz was suggested as a sensor for the medical fiberoptic OSL dosimetry system (Justus et al., 1999a). In the 1980s the OSL technique became popular in the archeological and geological dating community as a method of dose determination in natural materials like quartz and feldspar (see Huntley et al., 1985; Bøtter-Jensen et al., 2003).

Imaging phosphors like BaBrF:Eu (Sonada et al., 1983), Y_2SiO_5:Ce,Sm (Meijerink et al., 1991) barium phosphate doped with rare earth (RE) elements (Schipper et al., 1994), KBr:In (Trinkler et al., 1993) and imaging techniques based on their optical stimulation with lasers were successfully developed and some of them are now used in diagnostic digital radiography. Imaging plates based on europium activated barium and strontium fluoroholides (BaBrF:Eu, BaClF:Eu and $Ba_{(1-x)}Sr_x$ BrF:Eu) and readout systems are commercially produced by Fuji, Siemens, AGFA, Kodak, General Electric and other medical equipment manufacturers. The CR systems that are based in principal on the OSL technique show excellent imaging performance but are not capable of doing precise dosimetric measurements mostly because of low thermal stability of traps that results in relatively strong fading. Additional difficulties are caused by the high effective atomic number of BaBrF:Eu that is favorable for X-ray diagnostic imaging, but presents significant difficulties for precise measuring of doses in certain radiotherapy applications.

Another type of optically stimulated charge transfer process, known as phototransferred thermoluminescence (PTTL), was investigated in BeO (Tochilin et al., 1969), $CaSO_4$ (Pradhan and Ayyangar, 1977), CaF_2:Mn (Bernhardt and Herforth, 1974) and Al_2O_3:C (Miller et al., 1988; Yoder and Salasky, 1997) and suggested as a dosimetric tool. However, it did not became a useful technique because of practical difficulties and low sensitivity.

The ideal OSL material should satisfy several, sometimes conflicting characteristics. It should have deep thermally stable traps for long-term storage of dosimetric information without significant fading. At the same time, these traps should be optically accessible using light sources with wavelengths well separated from the emission bands of the recombination centers. This notion implies that there is no fundamental difference between TL and OSL materials. In general, all efficient dosimetric phosphors might exhibit both TL and OSL properties. The real advantage of some of the materials in comparison with the others is simply in the right combination of thermal and optical energy depths of the traps, in good separation between the emission and stimulation bands, and in a high photoionization cross-section of the traps. Single crystals of anion-deficient Al_2O_3:C, first developed as a highly sensitive TL material (Akselrod et al., 1990), appeared to well satisfy all these requirements and became widely used as an OSL detector.

Recently a new pulsed-OSL (POSL) technique for radiation dosimetry using anion-deficient Al_2O_3:C has been developed (Akselrod and McKeever, 1999) and is commercially implemented in LUXEL technology by Landauer Inc. In addition to efficient optical discrimination between stimulation and emission light using a combination of several optical filters, a time discrimination technique is used when the laser stimulation is pulsed and the OSL is measured only during the time between laser pulses. Studies of the OSL signal from Al_2O_3:C have shown it to be thermally stable and reproducible, with the detection of radiation gamma doses of 1 μGy possible. Optical bleaching may be used to "erase" the information from the material and to make it ready for the next use. Luminescent Al_2O_3:C material and an OSL technique are also used for imaging of radiation fields (Akselrod et al., 2000).

The versatility of the OSL technique allows one to use it in two different modes: a conventional *integrating mode*, wherein the OSL phosphor works as a passive detector and the interrogation with light takes place after the irradiation is over, and a *real-time mode* when stimulation with light is performed during irradiation and the information about both dose rate and total accumulated dose is acquired dynamically. Real-time OSL is a new approach in medical dosimetry and it has some clear advantages over well-known real-time radiation detectors like scintillators, Si-diodes, and MOSFET transistors. At the same time some challenges with OSL material engineering should be overcome to make real-time OSL a commercially viable dosimetry tool.

2. OSL theory

2.1. Stimulated luminescence

The absorption of energy from an ionizing radiation source by an insulating or semiconducting material causes the excitation of free electrons and free holes and the subsequent trapping of these electronic species at defects (trapping states) within the material. After removal of the excitation the sample may then be stimulated in such a way that absorbed energy causes the liberation of charge carriers of one sign, which are then able to recombine with charge carriers of the opposite sign. The radiation absorption and the excitation of charge (primarily by the Compton effect or the photoelectron effect, depending on radiation energy and type) lead to a perturbation of the system from a state of thermodynamic equilibrium to a metastable state. The subsequent absorption of external energy by the metastable trapped charge results in the stimulated relaxation of the system back to its equilibrium condition. During the relaxation process recombination of the electronic charge occurs and, if the recombination is radiative, luminescence is emitted. In OSL the stimulating energy source is light (UV, visible or infra-red).

OSL is one member of a family of stimulated relaxation phenomena (SRP). The intensity of the emitted luminescence is related to the rate at which the system returns to equilibrium. The rate at which the equilibrium is re-established is a function of the concentration of trapped (metastable) charge and in the simplest (first-order) case the rate is linearly proportional to the trapped charge concentration. Normally, one monitors the intensity of the luminescence as a function of time, resulting in a characteristic luminescence versus time curve. The integral of the luminescence versus time curve is thus related to trapped

charge, which, in turn, is proportional (in the ideal case) to the initial dose of the absorbed radiation. This is the basis for the use of OSL in radiation dosimetry.

2.2. Generalized mathematical description of OSL

The total concentration of occupied metastable states in the system at time t may be represented by $\mu(t)$, where

$$\mu(t) = \int_{\gamma_1}\int_{\gamma_2}\cdots\int_{\gamma_m} n(\gamma_1, \gamma_2, \ldots, \gamma_n, t)\,\mathrm{d}\gamma_1\,\mathrm{d}\gamma_2\cdots\mathrm{d}\gamma_m, \quad (1)$$

where $n(\gamma_1, \gamma_2, \ldots, \gamma_m, t)$ is the concentration of occupied states $1 \rightarrow m$, described by state parameters $\gamma_1, \gamma_2, \ldots, \gamma_m$, and in general $n(\gamma, t) = N(\gamma) f(\gamma, t)$. Here $n(\gamma)$ is the concentration of occupied states, $N(\gamma)$ is the concentration of available states, and $f(\gamma)$ is the occupancy of the state. ($f = 1$ when a state is full, and $f = 0$ when it is empty.) Both $n(\gamma)$ and $f(\gamma)$ are time-dependent functions.

The state parameters $\gamma_1, \gamma_2, \ldots, \gamma_m$ dictate the stability of the metastable state under the prevailing conditions of temperature and illumination intensity; that is they govern the probability per unit time that the system will return to equilibrium. $n(\gamma_1, \gamma_2, \ldots, \gamma_m, t)$ is a weighting function, or distribution, expressing the concentration of occupied states possessing the parameters $\gamma_1, \gamma_2, \ldots, \gamma_m$. Eq. (1) is a time-dependent and dose-dependent function since it increases during irradiation and decreases during stimulation.

In OSL the luminescence intensity I is proportional to the rate at which the metastable states decay, such that

$$I(t) = \left|\frac{\mathrm{d}\mu(t)}{\mathrm{d}t}\right|. \quad (2)$$

For *optical stimulation* of the trapped charge the probability p for optical stimulation at a given wavelength λ is

$$p(E_\mathrm{o}) = \Phi\sigma(E_\mathrm{o}), \quad (3)$$

where Φ is the optical stimulation intensity and $\sigma(E_\mathrm{o})$ is the photoionization cross-section for interaction of the metastable state with an incident photon, and E_o is the threshold optical stimulation energy required to release the charge and return the system to equilibrium. With reference to the terms given in Eq. (1) we can write that $m = 1$ and $\gamma_1 = E_\mathrm{o}$.

In the above representations λ and Φ are all fixed values independent of time. For optical stimulation, when the traps are emptied using a fixed wavelength λ and a steady illumination intensity Φ the luminescence recorded is known as *continuous wave OSL*, or CW-OSL. However, a time-dependence to p can be introduced by scanning the above terms with time—i.e. $\Phi(t)$ or $\lambda(t)$. Thus, for a linear increase in the intensity of optical stimulation at a fixed wavelength:

$$\Phi(t) = \Phi_\mathrm{o} + \beta_\Phi t, \quad (4)$$

with $\beta_\Phi = \mathrm{d}\Phi/\mathrm{d}t$. OSL recorded in this manner is known as *linear modulation OSL*, or LM-OSL. Other schemes can be imagined in which the intensity is modulated in non-linear ways.

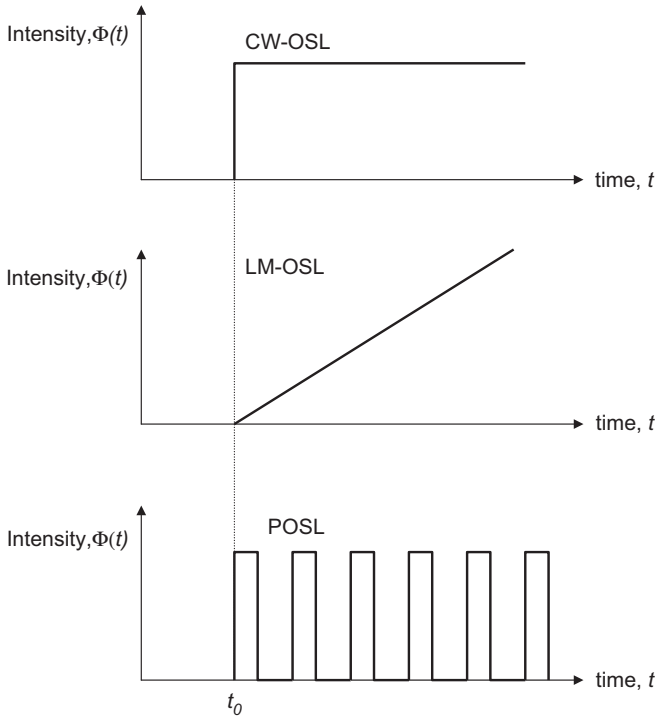

Fig. 1. Schematic representation of the three main OSL stimulation modes, namely: CW-OSL, LM-OSL and POSL.

For example, the stimulation may be pulsed, such that $\Phi(t) = \Phi_\mathrm{o}$ for $t_0 \leqslant t < t_0 + \Delta t$, and $\Phi(t) = 0$ for $t_0 + \Delta t \leqslant t < t_0 + \tau$, where Δt is the pulse width and τ is the period. Such a scheme is known as POSL. These various stimulation schemes are illustrated in Fig. 1.

2.3. The photoionization cross-section

The photoionization cross-section $\sigma(E_\mathrm{o})$ is perhaps the most important parameter dictating the stability of a particular trap during optical stimulation. The absorption coefficient for a defect-band optical transition at an optical stimulation energy $h\nu$ may be written as

$$\alpha(h\nu) = n(E_\mathrm{o})\sigma(h\nu, E_\mathrm{o}), \quad (5)$$

where $n(E_\mathrm{o})$ is the concentration of defects, each with an optical ionization threshold energy E_o. The dependence of the absorption coefficient $\alpha(h\nu)$ as a function of stimulation energy $h\nu$ should have an edge-like shape since the absorption line shape contains contributions from all the relevant continuum states in the band into which the electron is being excited (Stoneham, 1975). Following the transition, the charge on the defect will change by one electronic charge and significant lattice relaxation may occur. This is also true during the inverse process (Bräunlich, 1979).

Several expressions for the spectral dependence of $\sigma(E_\mathrm{o})$, namely $\sigma(h\nu, E_\mathrm{o})$, have been derived using a variety of assumptions relating to the potential energy in the vicinity of the defect. These are reviewed in some detail by Bøtter-Jensen et al.

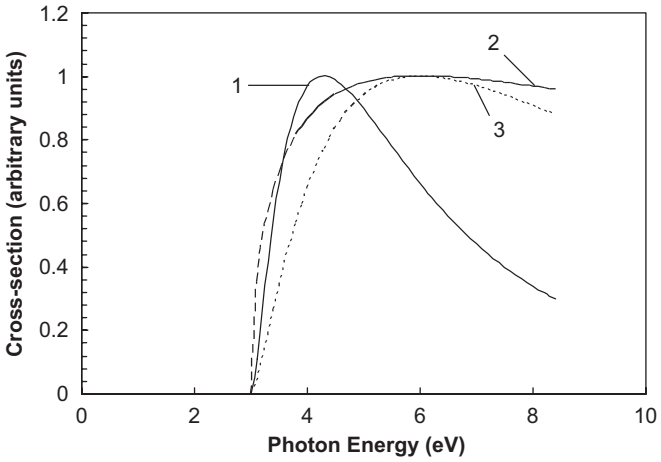

Fig. 2. Comparison of the shapes of various expressions for the photoionization cross-section as a function of stimulation photon energy, obtained with a threshold energy $E_o = 3.0\,\text{eV}$. Each curve is normalized to a maximum of 1. See Bøtter-Jensen et al. (2003) for full descriptions of the equations used to generate these curves.

(2003). The shapes of some of the functions for the photoionization cross-section are shown in Fig. 2 for a threshold energy of $E_o = 3.0\,\text{eV}$, and $m_o/m_e = 2$. For each curve, $\sigma = 0$ for $h\nu \leqslant E_o$. The threshold optical ionization energy E_o is larger than the thermal ionization energy (thermal trap depth, E_t) by an amount equal to the phonon energy, namely

$$E_{ph} = S\hbar\omega_p, \tag{6}$$

where S is the Huang–Rhys factor and ω_p is the phonon vibration frequency (Bøtter-Jensen et al., 2003).

2.4. CW-OSL

The transitions of charge between energy levels during irradiation and subsequent optical stimulation of a dosimeter can be described by a series of non-linear, coupled rate equations of the type given generically in Eqs. (1) and (2). The equations themselves are intractable and several simplifying assumptions have to be introduced in order to arrive at analytical expressions for the evolution of the OSL intensity with time during optical stimulation and, ultimately, the dependence of the OSL signal on the absorbed dose. Several energy-level models can be imagined on which to base these analyses, and each includes transport of electrons through the conduction band in order for them to reach the trapped holes at the radiative recombination sites. The simplest is that corresponding to a system containing one type of electron trap and one type of hole trap (the one-trap/one-center model). The trapped holes act as recombination centers at which recombination of electrons with the holes occurs, leading to the emission of luminescence. Additional complexities can be introduced in a systematic fashion to gain an appreciation of the role played by additional electron traps and/or recombination centers. These models are explored in the following sections.

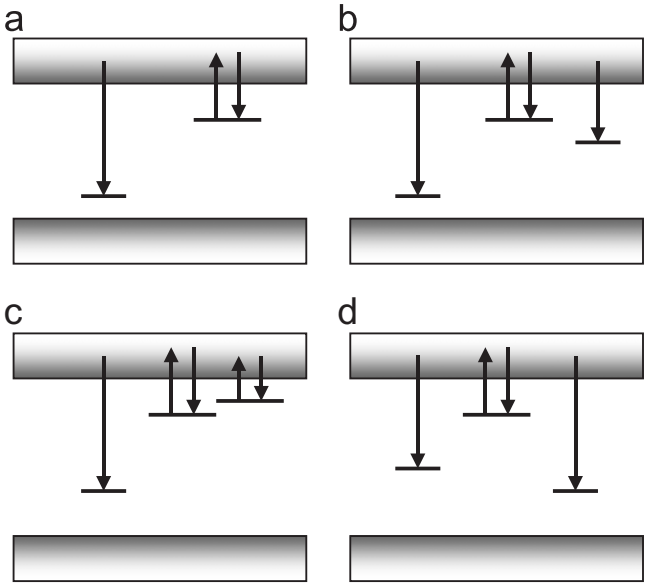

Fig. 3. Simple models for OSL. (a) Simplest model; involving one trap and one radiative recombination center. (b) Model containing an additional deep, competing trap. (c) Model containing a shallow, competing trap. (d) Model containing a competing non-radiative recombination center.

2.4.1. The one-trap/one-center model

The model is shown in Fig. 3(a). Charge neutrality for this system can be written as

$$n_c + n = m_v + m, \tag{7}$$

where n_c and n are the concentrations of electrons in the conduction band and the traps, respectively, and m_v and m are the concentrations of holes in the valence band and hole traps (recombination centers), respectively. If we consider thermal equilibrium at the end of the irradiation period such that n_c and m_v are zero, then we may write that at the start of optical stimulation $n_0 = m_0$, where the subscripts "0" imply at time $t = 0$.

During optical stimulation of the electrons from the traps transitions to the valence band do not occur and at any time t during the optical stimulation period the charge neutrality condition becomes $n_c + n = m$ from which we may write the rate of change of the various concentrations as

$$\frac{dn_c}{dt} = -\frac{dn}{dt} + \frac{dm}{dt}. \tag{8}$$

The terms on the right-hand side may be written explicitly as

$$\frac{dn}{dt} = np - n_c A(N - n) \tag{9}$$

and

$$\frac{dm}{dt} = n_c A_m m = \frac{n_c}{\tau}. \tag{10}$$

Here, p is the rate of stimulation (in units of s^{-1}) of electrons from the trap and is related to the incident photon flux Φ and the photoionization cross-section σ by

$$p = \Phi\sigma, \tag{11}$$

as already seen in Eq. (3) and where the dependence on wavelength is understood for a given optical ionization threshold energy. The other terms in Eqs. (8) and (9) include: A, which is the trapping probability (in units of $m^3\,s^{-1}$); A_m, which is the recombination probability (also in units of $m^3\,s^{-1}$); N, which is the total available concentration of electron traps (in m^{-3}); and $\tau = 1/A_m m$, which is the free electron recombination lifetime (in s). With the introduction of a quasi-stationary population of free electrons in the conduction band (the so-called "quasi-equilibrium approximation", or $dn_c/dt \ll dn/dt, dm/dt$ and $n_c \ll n, m$) we have

$$\frac{dm}{dt} = \frac{dn}{dt}. \tag{12}$$

The second major assumption to be introduced at this point is that of slow retrapping, that is, $n_c A(N-n) \ll np, n_c A_m m$. This leads to

$$I_{OSL} = -\frac{dm}{dt} = -\frac{dn}{dt} = np, \tag{13}$$

the solution of which is

$$I_{OSL} = n_0 p \exp\{-tp\} = I_0 \exp\{-t/\tau_d\}. \tag{14}$$

Here, I_0 is the initial OSL intensity at $t = 0$, and τ_d is the CW-OSL decay constant. This first-order model leads then to an exponentially decaying OSL intensity as the (constant) stimulation light intensity is applied to the sample. Eventually, all the traps are depleted and the OSL becomes zero (McKeever et al., 1997).

This simple result (i.e. an exponential decay of OSL during stimulation with a fixed intensity stimulation beam, Eq. (14)) is obtained under the stringent conditions of slow retrapping, or first-order kinetics (cf. $dn/dt = -np$). In practice, however, experimental CW-OSL decay curves show a wide variety of curve shapes that do not conform to this simple exponential description. An obvious cause for such deviation from this simple rule may be the addition of other optically active traps leading to two or more electron traps releasing their trapped charge at the same time, each at its own rate and described by its own photoionization cross-section at the stimulation wavelengths used. Even with the one-trap/one-center model, however, non-exponential OSL curves can be obtained, as described in full in McKeever (2001) and Bøtter-Jensen et al. (2003).

The decay constant and the trap emptying rate are related to the photoionization cross-section by $\tau_d^{-1} = p = \Phi\sigma$. For a sample that is stimulated by a narrow band of monochromatic light (for example, from a laser) then the decay constant will be single-valued. Some popular OSL systems used in modern experiments use a band of stimulation wavelengths. Since both Φ and σ vary with wavelength, a range of values for $p = \tau_d^{-1}$ will result. However, a single exponential decay is still expected with the decay constant now given by $\tau_d^{-1} = \int \sigma(\lambda)\Phi(\lambda)\,d\lambda$ and the evaluated effective decay constant is the mean of the distribution of decay constants caused by the broad band stimulation. A potentially more serious problem occurs when the intensity of the stimulation light is spatially distributed non-uniformly over the surface of the sample (e.g. the TEM_{00} mode from a laser). Since now different parts of the sample are experiencing different intensities (albeit at the same wavelength) the net result again is that the measured decay constant τ_d may not be single-valued.

2.4.2. Models containing multiple-traps and centers

For two optically sensitive traps, of trapped charge concentrations n_1 and n_2 and with stimulation rates $p_1 = \tau_{d1}^{-1}$ and $p_2 = \tau_{d2}^{-1}$, it is straightforward to show (McKeever et al., 1997) that

$$\frac{dm}{dt} = -\frac{dn_1}{dt} - \frac{dn_2}{dt}, \tag{15}$$

and that

$$\begin{aligned} I_{OSL} &= n_{10} p_1 \exp\{-tp_1\} + n_{20} p_2 \exp\{-tp_2\} \\ &= I_{10} \exp\{-t/\tau_{d1}\} \\ &= I_{20} \exp\{-t/\tau_{d2}\} \end{aligned} \tag{16}$$

using the superposition principle and no interaction between the traps. Clearly, this can be extended to three or more optically sensitive traps, each emptying at their own characteristic rate during stimulation.

Extending this to a distribution of traps (Whitley and McKeever, 2000) with a distribution of threshold energies E_o and stimulation photon energy $h\nu$, we may write

$$\begin{aligned} I_{OSL}(h\nu) &= \int w(E_o)\, p(h\nu, E_o)\, dE_o \\ &= \Phi(h\nu) \int w(E_o)\sigma(h\nu, E_o)\, dE_o, \end{aligned} \tag{17}$$

where $w(E_o)$ is a weighting factor defining that fraction of the OSL curve that is due to a particular trap.

If the additional traps introduced into the energy band model are not sensitive to the optical stimulation, they can still act as traps for released charge and affect the OSL decay kinetics. An example is shown in Fig. 3(b) where we see a deep trap able to capture free charge but from which optical stimulation does not occur. (One can imagine, for example, stimulation with long wavelength light optically emptying shallow traps but with the light being of insufficient energy to empty the deep traps.) In this model the deep traps may be viewed upon as competitors to the recombination centers.

The OSL intensity in this case is described by

$$I_{OSL} = n_{10} p \exp\{-t/\tau\} - n_c A_2 (N_2 - n_2), \tag{18}$$

where N_2, n_2 and A_2 are the concentration of available traps, concentration of filled traps, and trapping probability, respectively, for the deep trap. Thus, the OSL intensity is reduced by an amount dictated by the relative rates of recombination and trapping into the deep, competing trap. The decay is no longer exponential since the second term in Eq. (18) is time-dependent and approaches zero as $t \to \infty$.

If the competing centers are shallow (Fig. 3(c)):

$$\begin{aligned} I_{OSL} = {} & n_{10} p \exp\{-t/\tau_d\} + n_2 s \exp\{-E/kT\} \\ & - n_c A_2 (N_2 - n_2), \end{aligned} \tag{19}$$

where s and E are the pre-exponential factor and thermal trap depth for the shallow trap, and k is Boltzmann's constant. The last two terms in Eq. (19) combine to produce a long-lived, temperature-dependent component to the OSL decay curve. The form of this component is an initial increase, followed by a decrease at longer times. Depending on the size of the first term compared with the second and third terms the overall OSL intensity can also exhibit an initial increase followed by a decrease. In such circumstances the terms "OSL decay curve" is inappropriate. Key elements are the intensity of the stimulation light p, and the temperature T, such that at certain combinations of p and T the initial increase may be observed, whereas for other combination only a decay may be observed.

A further example of energy levels in the OSL model is obtained by considering a second recombination center such that the total trapped electron concentration n after irradiation is given by $n = m_1 + m_2$. Here, m_1 and m_2 are the concentrations of trapped holes in the two recombination centers, respectively. With the assumption that only electron–hole recombination in the first center is radiative (thus, $I_{OSL} = -\mathrm{d}m_1/\mathrm{d}t$) and that recombination at the second center is non-radiative (or, if radiative, is outside the detector sensitivity window) we have

$$I_{OSL} = np \exp\{-t/\tau_d\} - \frac{\mathrm{d}m_2}{\mathrm{d}t}, \tag{20}$$

where we again see that the OSL intensity is reduced by the presence of a non-radiative pathway for charge interaction. Under the circumstances that the recombination probabilities are similar (Bøtter-Jensen et al., 2003) the CW-OSL decay curve remains approximately exponential according to

$$I_{OSL} = \frac{1}{K} n_0 \, p \exp\{-tp\}, \tag{21}$$

where K is a constant given by $K = (m_1 + m_2)/m_1$.

2.4.3. A model for Al_2O_3

The above analyses are for certain very special cases only. In the models we have discussed we have assumed (say) a shallow trap, *or* a deep trap, *or* a second recombination center. Real materials, however, contain multiple traps and centers, some of which may be shallow, some of which may be "optically sensitive" (i.e. the charge may be optically stimulated from the trap at the wavelength being used), some of which may be deep. Some of the recombination centers may be radiative, and others not. Charge transfer effects may take place between some centers, and not others. The charge transfer processes may involve the conduction band (as is assumed so far) or they may not. In other words, real materials show a complexity of behavior which is far greater than that indicated so far in this text.

A first step toward a more realistic model for a real OSL material, and one that is especially appropriate for Al_2O_3, was discussed by Polf et al. (2004) and Yukihara et al. (2004a) and is shown in Fig. 4. Here, transition (1) represents ionization (electron–hole pair creation) due to absorption of radiation. Transition 2a represents hole trapping and a recombination site and 2b is the recombination transition. The OSL signal

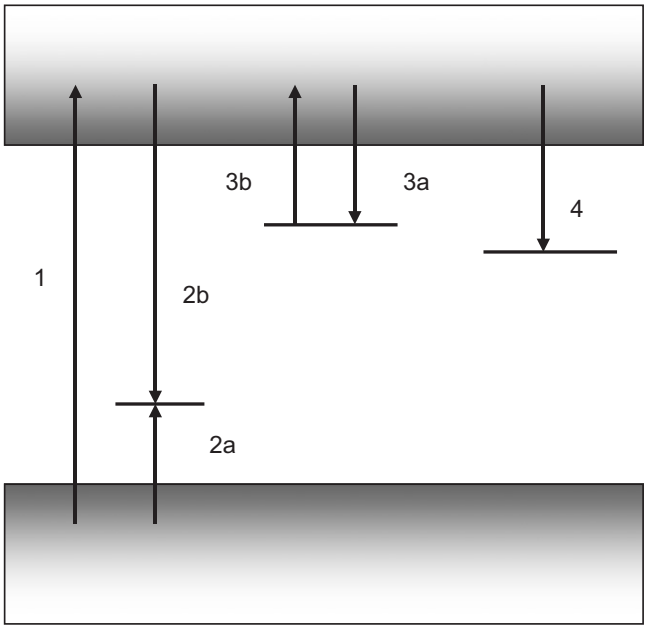

Fig. 4. A more complex model for simulation of real-time OSL detection (from Polf et al., 2004; Yukihara et al., 2004a,b).

originates from trapping of an electron in the dosimetry trap 3a, and 3b is the optical stimulation transition. The final transition (4) is a capture of electrons by deep traps. Normally one considers that the concentration of recombination centers increases with dose due to trapping transition 2a. However, in Al_2O_3 the recombination centers are F^+-centers (oxygen vacancy centers with one electron; see Section 3). During irradiation, transition 2b dominates because of the pre-existing F^+ concentration. Thus, at high enough doses, the recombination center concentration actually decreases with dose, as was demonstrated by Yukihara et al. (2003).

The effect of this, in combination with the effect of deep traps, on the OSL (and TL) behavior is quite profound. Fig. 5 shows the results of a numerical simulation of the TL and CW-OSL curves as a function of dose. It is clear that the TL peak shifts to lower temperatures and the OSL peak decays more quickly as the dose increases. Both of these effects are seen experimentally, as is shown in Fig. 6 for OSL from Al_2O_3 as a function of beta dose. An additional effect is that the OSL decreases at very high doses as the sensitivity of the sample is reduced. Typical data are shown in Fig. 7. Such data are important in predicting the response OSL from this material in heavy charged particle irradiation, as one may find in certain radiotherapy applications.

2.4.4. Real-time OSL: computer simulations

Continuing with this model, Polf et al. (2004) predicted how such a system would behave during *real-time* OSL measurements. The procedure for real-time OSL involves the periodic "pulsing" of the optical stimulation simultaneously with the irradiation, while continually monitoring the luminescence emission. Note that although the stimulation is pulsed, the OSL monitored is CW-OSL—that is the OSL is monitored during the

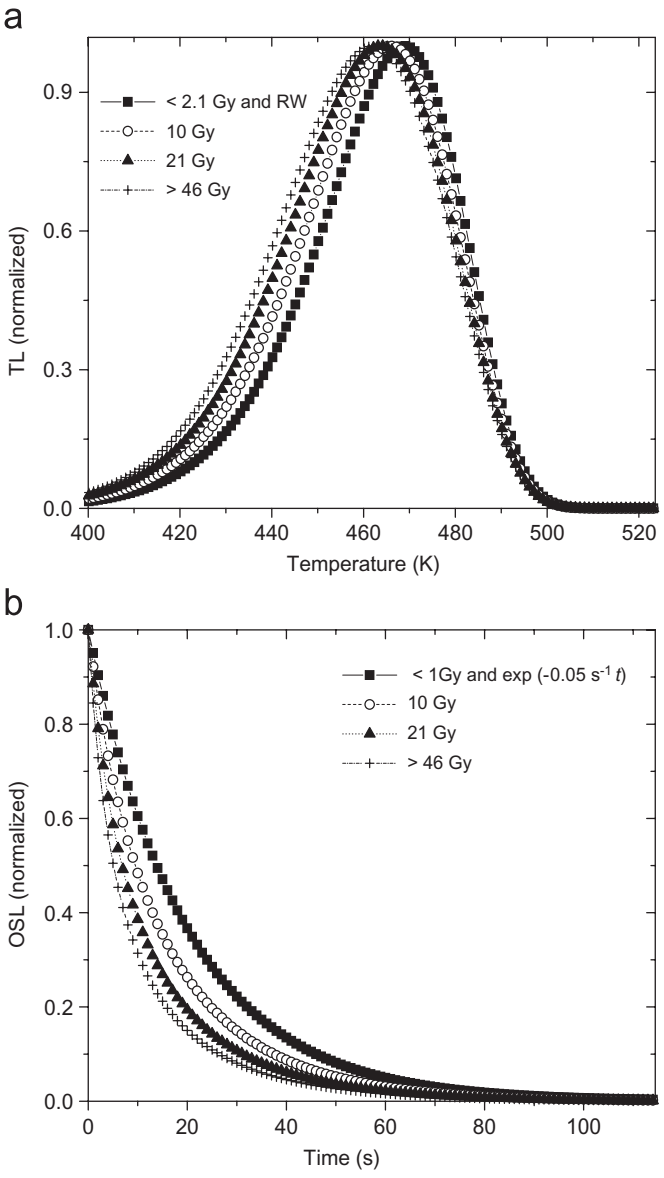

Fig. 5. (a) TL curves and (b) OSL curves generated by numerically solving the rate equations appropriate to the model of Fig. 4, for various doses (from Yukihara et al., 2004a).

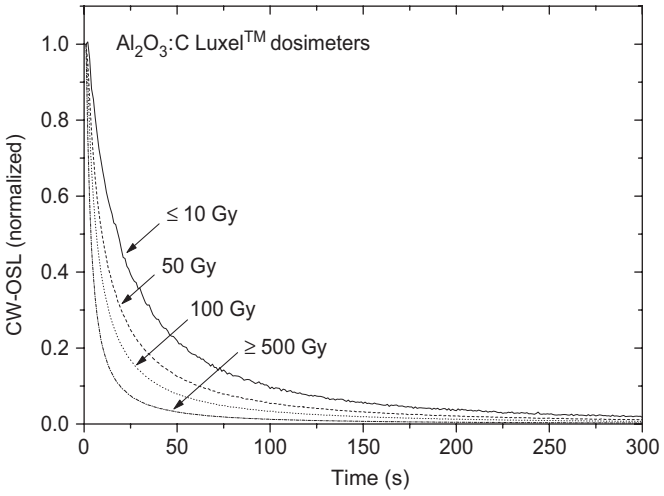

Fig. 6. Normalized CW-OSL curves for different beta doses (from Yukihara et al., 2004b).

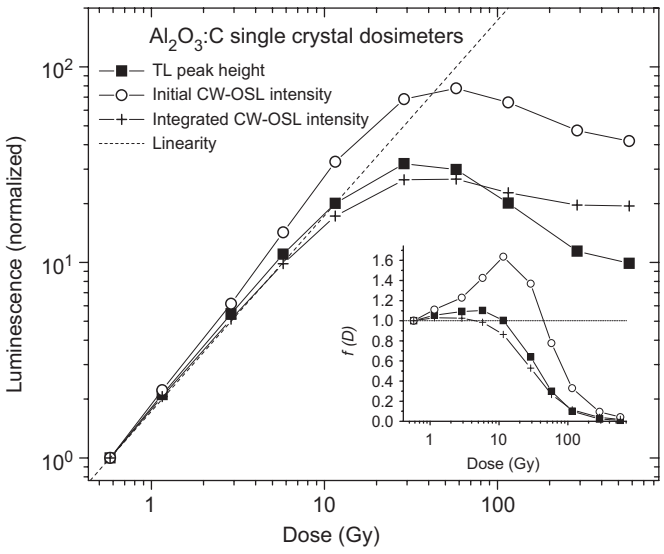

Fig. 7. CW-OSL (and TL) versus dose curves from Al_2O_3 irradiated with beta irradiation (from Yukihara et al., 2004b).

optical stimulation, the period of which is longer than the lifetime of the intrinsic luminescence emission (35 ms in Al_2O_3). Since the luminescence emission is continually monitored, radioluminescence (RL) is measured in those periods between the pulses, while OSL + RL is monitored during the stimulation periods (Fig. 8). By subtraction, the OSL-only signal can be extracted.

The situation is demonstrated by the numerically simulated data of Fig. 9. In (a) is shown the background RL signal between the stimulation pulses, and the OSL+RL signal during the short stimulation pulses. A number of observations are to be made. Firstly, the RL background is not constant and increases with irradiation time, the cause of which is trap filling. As the traps fill, so the RL intensity increases since the trap filling represent a competing pathway to electron–hole recombination at the F^+-centers. (At very long irradiation times, the RL intensity decreases again due to removal of F^+-centers, as discussed above.) Similarly, the OSL intensity shows a strong rise to a steady-state level (see both (a) and (b)). The steady-state level is achieved when the loss of trapped charge caused by each stimulation pulse equals the increase in trapped charge due to the irradiation between pulses. The steady-state level itself is dictated by the laser power used, the width of the stimulation pulse, and the dose rate (Polf et al., 2004).

The effect of deep and shallow traps on the rise to steady state is demonstrated in Fig. 10. The primary effect is to slow the rise, both for RL and OSL. An additional effect of deep and shallow traps is to slow the OSL decay. This occurs for

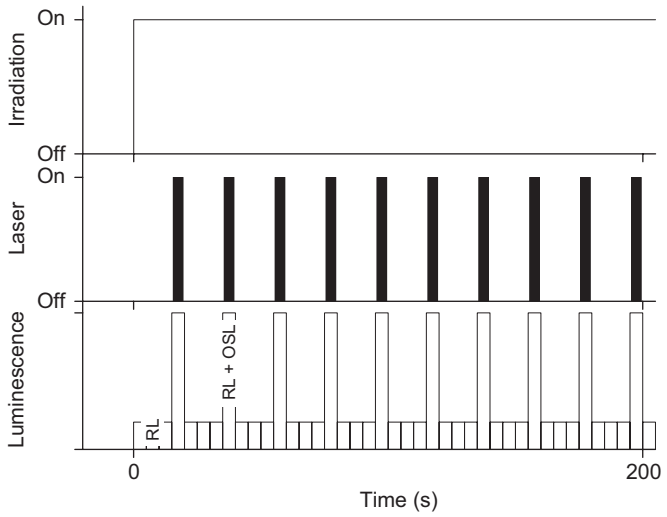

Fig. 8. The irradiation, laser stimulation and light detection scheme employed during real-time assessment of dose using OSL (from Polf et al., 2004).

two reasons. First, the deep traps can also be emptied by optical excitation but, since they are deeper than the dosimetry traps, the rate of trap emptying (given by Eq. (3)) is lower at a given wavelength. This gives rise to a long tail in the OSL decay curve. Furthermore, since charge accumulates in the deep traps during the irradiation period, the relative size of this tail increases with irradiation time. The second cause of the slowdown of the OSL decay is retrapping of optically freed electrons by the shallow traps. Although the shallow traps in Al_2O_3 are only partially optically active (i.e. they do not readily empty during optical stimulation; Polf et al., 2004) they do empty thermally since they have small thermal activation energies. Thus, charge retrapped by shallow traps leads to an optically stimulated phosphorescence signal that initially increases with stimulation time, and then decreases (McKeever et al., 1997; Bøtter-Jensen et al., 2003).

3. Experimental considerations

3.1. Defect properties in sapphire

α-Al_2O_3 has a rigid, slightly distorted, hexagonal-close-packed O^{2-} sublattice with Al^{3+} ions occupying two out of every three octahedral interstices. Each Al^{3+} ion is surrounded by six octahedral nearest-neighbor O^{2-} ions. (Fig. 11). As indicated in Section 2, the primary information storage process in Al_2O_3 is that of electronic ionization, followed by the subsequent capture of the excited electronic charge by trapping centers. Thus, for the efficient storage of dosimetric information, it is necessary that Al_2O_3 crystals should contain several species of defects trapping electronic charge carriers of both polarities. The efficient production of luminescence, however, requires not just a high concentration of trapping sites—it also requires efficient radiative recombination pathways for electrons and holes, producing photons.

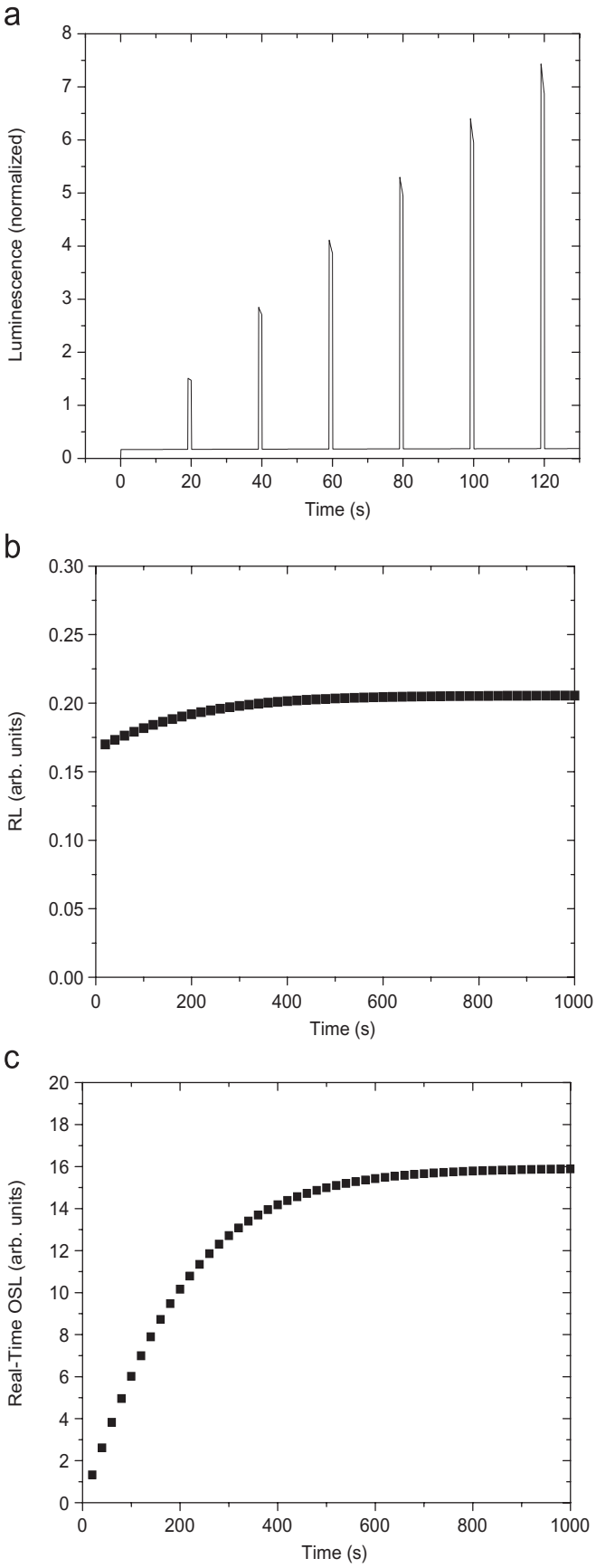

Fig. 9. Simulated detected luminescence (a), RL (b) and OSL (c) using the scheme shown in Fig. 8 and the model of Fig. 4 (from Polf et al., 2004).

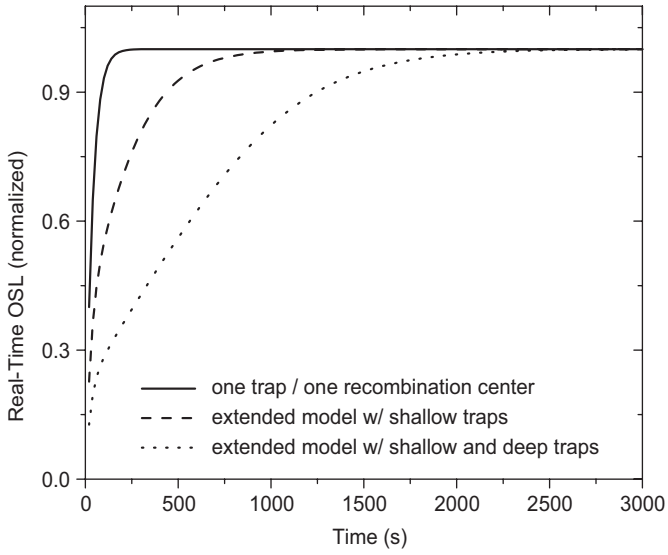

Fig. 10. The simulated growth of OSL versus irradiation time for the model of Fig. 4, with and without deep and shallow traps (from Polf et al., 2004).

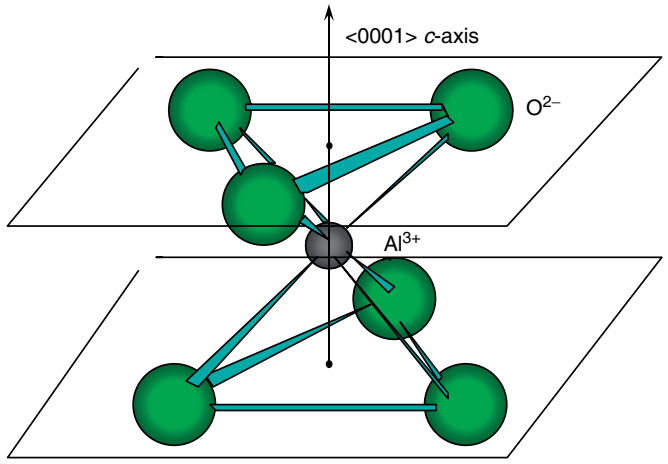

Fig. 11. Simplified crystal structure of Al_2O_3.

3.2. Historical overview of Al_2O_3 in radiation dosimetry

Point defects in the form of oxygen and aluminum vacancies (F- and V-type centers, respectively) and different impurities have been exploited in the various forms of α-Al_2O_3, which was introduced as a TLD dosimeter since the early 1950s. Ti-doped Al_2O_3 single crystals were first suggested as a TLD material by Rieke and Daniels (1957) and further investigated by Buckman (1972) and McDougall and Rudin (1970). Ceramic Al_2O_3 pellets doped with Si and Ti and processed in an oxygen–acetylene flame was reported by Mehta and Sengupta (1976). Osvay and Biro (1980) made an extensive study of ceramic TLD pellets made of Al_2O_3:Mg,Y, Cr-impurity was tried by Lapraz et al. (1988) and a combination of two impurities Cr and Ni in Al_2O_3 was investigated by Pokorny and Ibarra (1994).

However, aluminum oxide was not sensitive enough as a luminescent material until the introduction of anion-deficient and carbon-doped aluminum oxide (Al_2O_3:C). Al_2O_3:C was developed first as an ultra-sensitive TLD in the late 1980s (Akselrod et al., 1990) and is now considered as a sensitive and practical OSL material (McKeever et al., 1996; Akselrod and McKeever, 1999). It has a linearity of light output as a function of radiation dose of 7 orders of magnitude, no fading of the information due to the deep nature of the traps and extremely good environmental stability. The long luminescence lifetime (35 ms) of the F-centers in this material was successfully exploited in time-discrimination technique of POSL (Akselrod and McKeever, 1999).

3.3. Crystal growth, defect formation and luminescence centers in Al_2O_3:C

Al_2O_3:C crystals are grown using the Stepanov technique in a highly reducing atmosphere at a low partial pressure of oxygen. Under such conditions stable oxygen vacancies are created by the process of "subtractive coloration". Occupancy of an oxygen vacancy by two electrons gives rise to a neutral F-center, whereas occupancy by one electron forms a positively charged, with respect to the lattice, F^+-center. These centers can be identified by strong absorption bands at 205 nm assigned to F-centers (Lee and Crawford, 1977) and two overlapping absorption bands at 230 and 255 nm assigned to transitions in F^+-centers (Evans and Stapelbroek, 1978). Oxygen vacancy defects can also be produced in Al_2O_3 crystals by neutron and high-energy electron irradiation and also by thermochemical reduction (additive or subtractive coloration). F- and F^+-centers are known to play a key role in the high luminescent output (TL and OSL) of Al_2O_3.

F-centers produce luminescence at 420 nm with long (35 ms) lifetime, whereas F^+-center emission is centered at 330 nm and has extremely short lifetime (< 7 ns). It was found that an increase in the concentration of F^+-centers in Al_2O_3:C causes significant increase in OSL and TL sensitivity. It was suggested that oxygen vacancies in the form of F^+-centers are created in Al_2O_3 doped with carbon during crystal growth in highly reducing atmosphere as a result of charge compensation of divalent carbon ion substituting trivalent Al^{3+}-ion (Akselrod et al., 1990). One of the possible configurations of this defect is depicted in Fig. 12. It is important to mention the effect of thermal quenching of F- and F^+-center luminescence that reduces the yield of TL in Al_2O_3 at a high heating rate. Evans and Stapelbroek (1978) showed this effect for F^+-centers and Akselrod et al., 1998b for F-centers. The OSL process is not affected by thermal quenching, however, resulting in a significant gain in light output in comparison with TL (McKeever and Moscovitch, 2003).

3.4. Dosimetric properties of Al_2O_3:C for OSL applications

The reason for the success of Al_2O_3:C as a practical OSL radiation detector material is in the unique combination of several important parameters, but there is no doubt that other materials may be synthesized in the future with even better

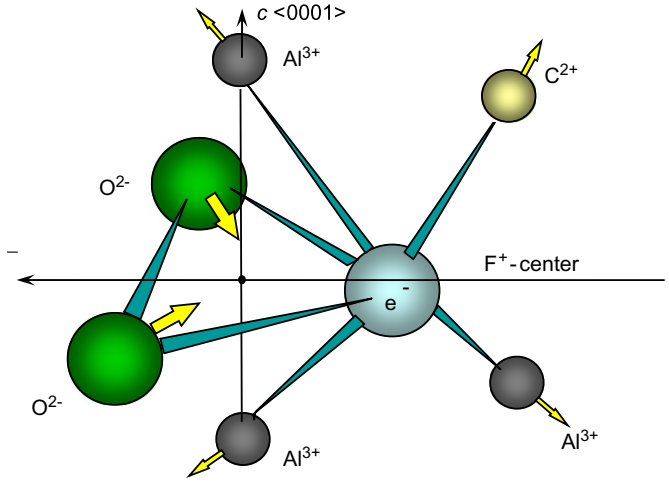

Fig. 12. Suggested configuration of an F^+-center charge-compensated by a divalent carbon ion.

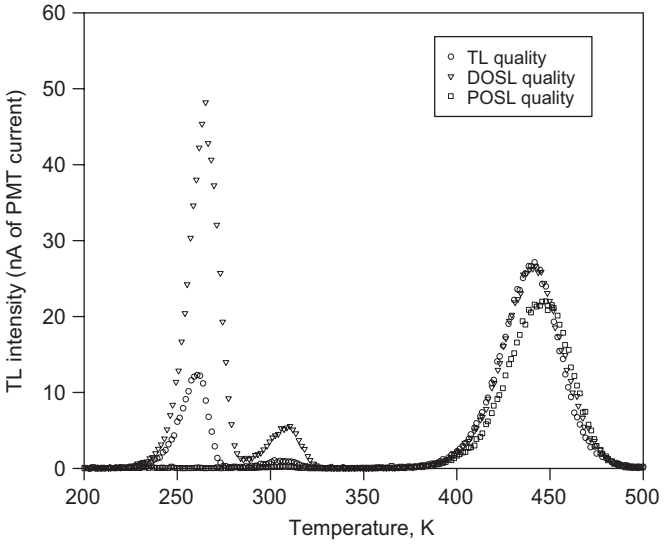

Fig. 14. TL curves of Al_2O_3:C crystals of three different quality (TL, DOSL and POSL) obtained after gamma irradiation with a ^{137}Cs source at liquid nitrogen temperature.

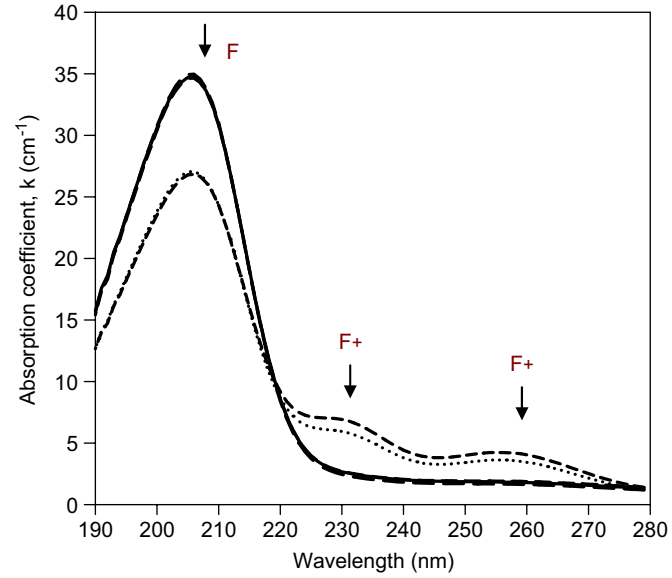

Fig. 13. Optical absorption spectra of Al_2O_3:C crystal indicating absorption bands of F- and F^+-centers and their transformation after irradiation, bleaching with light, and thermal annealing.

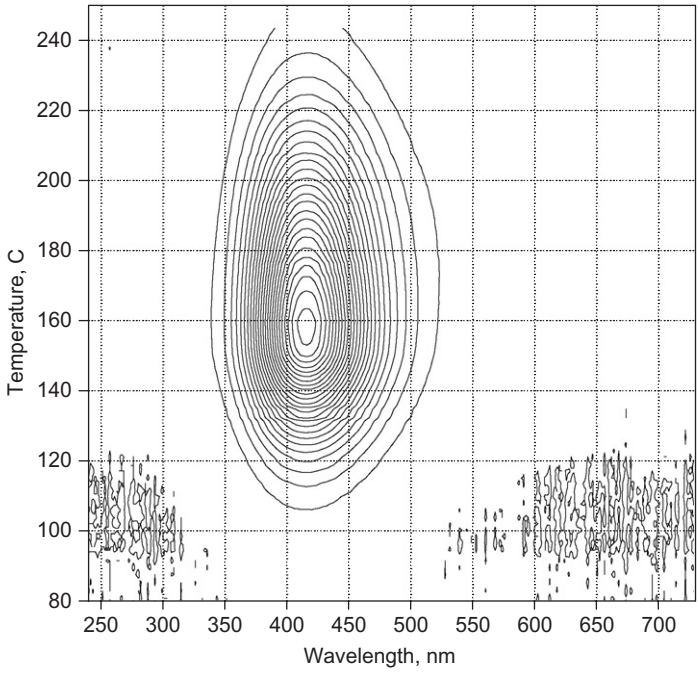

Fig. 15. Contour plot of TL emission from Al_2O_3:C crystal at low 0.1 K/s heating rate.

dosimetric performance. The main fundamental advantage of Al_2O_3:C as a radiation detector is that it has a wide (9.5 eV) energy band-gap, allowing one to engineer deep and thermally stable traps and color centers. Optical absorption bands at 205, 230 and 255 nm (Fig. 13) assigned to F- and F^+-centers show high concentrations of oxygen vacancies in Al_2O_3:C crystals. Phototransformation of F- and F^+-centers during irradiation, bleaching and annealing to different temperatures allows one to determine the type of charge carriers participating in TL, OSL and phototransfer process (Yukihara et al., 2003).

The dosimetric TL peak in Al_2O_3:C measured at a heating rate of 5 K/s is located at about 450 K (Fig. 14). Thermal activation energy obtained from TL peak analysis is estimated around 1.5 eV. The electron trap associated with this TL peak is very stable at temperatures close to room temperature with a measured fading rate of less than 5% per year. At the same time the optical depth of this trap is not very large and is equal to 2.75 eV (450 nm). This determines the range of wavelengths suitable for optical stimulation (Colyott et al., 1996). Although the most efficient wavelength for OSL stimulation of Al_2O_3:C is in the blue (Whitley and McKeever, 2000), a need to discriminate the stimulation light from the broad F-center emission centered at 420 nm (Fig. 15) determines the use of green

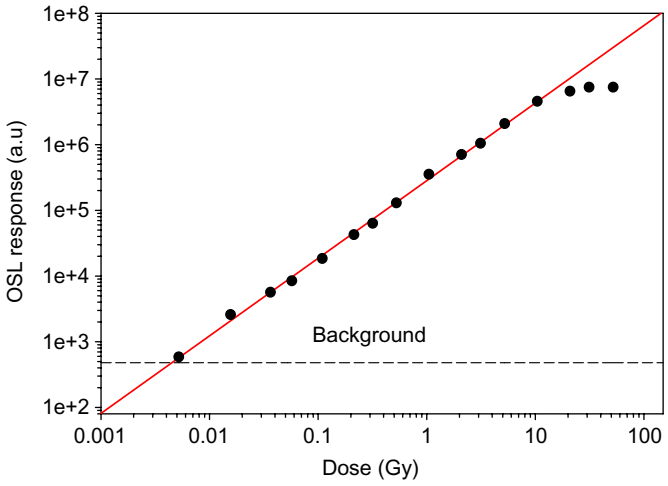

Fig. 16. Dose dependence of OSL signal from an Al_2O_3:C fiber.

stimulation with sources of light like the 532 nm second harmonic of a Nd:YAG laser, the 514 nm line of an Ar-ion laser or InGaN LEDs with a peak wavelength at 520 nm. In practical OSL readers single photons of luminescence are detected in the presence of up to 10^{22} photons of stimulation light and good optical separation and filtration is required.

A high sensitivity to radiation (determined as a number of emitted luminescence photons per unit of absorbed dose), a wide range of linearity of dose dependence (Fig. 16), a low background signal under optical stimulation, and an acceptable photoionization cross-section of traps at the chosen wavelength are among the important dosimetric parameters of Al_2O_3:C. Al_2O_3:C is an erasable OSL material and can be reused multiple times after optical bleaching or thermal annealing. Bleaching kinetics are not first-order, and the OSL decay is not described by a single-exponential. This is probably a result of relatively wide distribution of optical activation energies (Whitley and McKeever, 2000). Filling of deep traps during high dose irradiation can create some difficulties when performing complete optical bleaching and may require high-temperature annealing to completely zero the detector and so reduce the background OSL signal from the deep traps.

It has been shown that the same traps in Al_2O_3:C are responsible for both OSL and TL production. The single TL peak at about 450 K is produced after gamma-irradiation and UV excitation (although the TL peak shape after UV irradiation is not the same as that after irradiation with gamma). Two shallow traps, responsible for TL peaks at 260 and 310 K, have also been reported. The existence of both shallow and deep traps in Al_2O_3:C affects the performance of the material as an OSL detector. For example, shallow traps in different types of Al_2O_3:C developed for TL, OSL and "delayed" OSL (DOSL) applications were investigated using the TL technique after irradiation at liquid nitrogen temperatures (Fig. 14). Retrapping of delocalized charges in the shallow traps reduces the probability of radiative recombination and slows the OSL decay. Shallow traps also introduce a temperature dependence to the OSL measurements such that different OSL decay curve shapes are obtained if stimulated at different temperatures (Akselrod et al., 1998a).

The existence of several efficient deep traps with delocalization temperatures at approximately 680, 770, 920 and 1170 K were identified using methods of PTTL (Akselrod and Gorelova, 1993), high-temperature TL (Molnar et al., 2002) and photoconductivity (Whitley and McKeever, 2000). One of the ways to determine the thermal energy ("depth") of the deep traps is to measure TL after high-temperature irradiation, as depicted in Fig. 17 (see Molnar et al., 2002). Deep traps affect the OSL process in different ways. Firstly, they compete for charge carriers during irradiation. This in turn causes changes in the OSL sensitivity as the deep traps are filled during the irradiation period. Whether the sensitivity increases or decreases as the deep traps fill depends upon whether the deep traps are holes traps, or electron traps, both of which are known to exist in this material. Yukihara et al. (2004a) demonstrated that in some samples the hole traps dominate and thus the sensitivity is smaller after deep trap filling compared with when all traps are empty. Conversely, in samples in which the deep electron traps dominate over the deep hole traps, the sensitivity increases with deep trap filling. Secondly (as already noted), the deep traps (specifically the electron traps) are responsible for a residual OSL signal that is difficult to eliminate using optical bleaching when using stimulation wavelengths normally used in OSL measurement.

Another important feature of OSL using Al_2O_3:C is its ability to be reliably re-read. Thus, the dose may be independently measured multiple times from the same detector. This arises from the high sensitivity of the method such that each OSL measurement only empties a fraction of the trapped charge available. The accumulated amount of charge on the dosimetry traps is so large that it is possible to precisely read the dose using only 2–3% of the total OSL signal. Depletion kinetics remain constant for the low dose range (up to 5 Gy) and allow one to perform precise dose re-estimation, after correction for partial trap depletion (Akselrod and McKeever, 1999).

3.5. *Al_2O_3:C fibers for remote OSL dosimetry*

Modern crystal growth techniques allows one to obtain α-Al_2O_3:C single crystal fibers that may be suitable for *in vivo* and/or *in vitro* medical applications in radiation dosimetry. As in the case of regular Al_2O_3:C material crystal growth of Al_2O_3:C fibers is performed using the Stepanov process in a highly reducing atmosphere and a low partial pressure of oxygen ($\sim 10^{-20}$ atm). Single crystal fibers of several diameters 300, 500, 1000 and 2000 μm have been obtained. The grown fibers may be cut into pieces of different lengths. Typical lengths are: 0.2, 0.5, 1, 3, 6 and 9 mm. The cut fibers may be polished on both ends to obtain optical quality surfaces for investigation and further coupling with silica fiberoptic cables.

For a high spatial resolution, fiber probes with diameters and lengths less than 500 μm are needed. In the Stepanov crystal growth process the shaping unit determines the diameter and the cross-sectional shape of the single crystal fiber pulled from

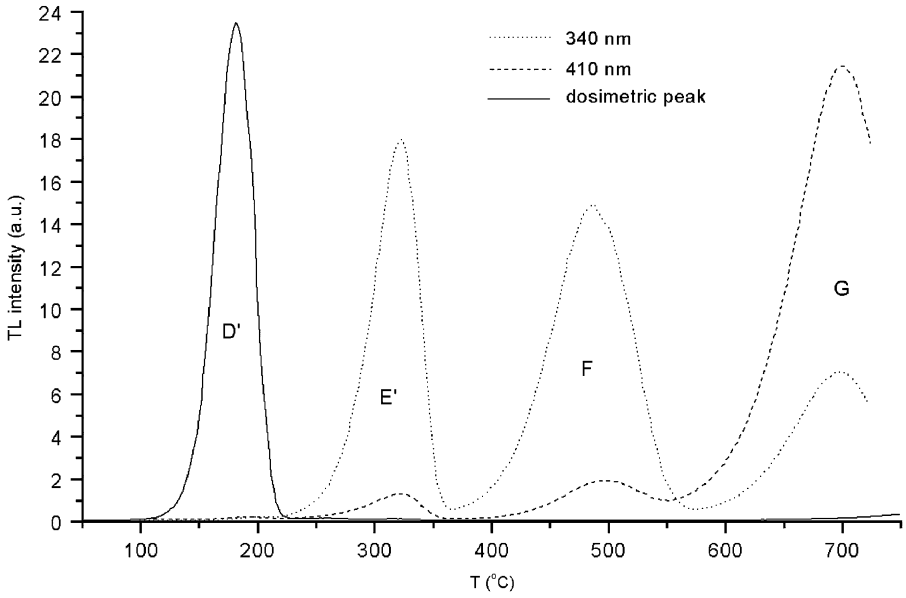

Fig. 17. Deep traps in Al_2O_3:C indicating themselves as TL peaks obtained after 205 nm UV illumination at elevated temperature and measured through 340 and 410 nm interference filters (from Molnar et al., 2002).

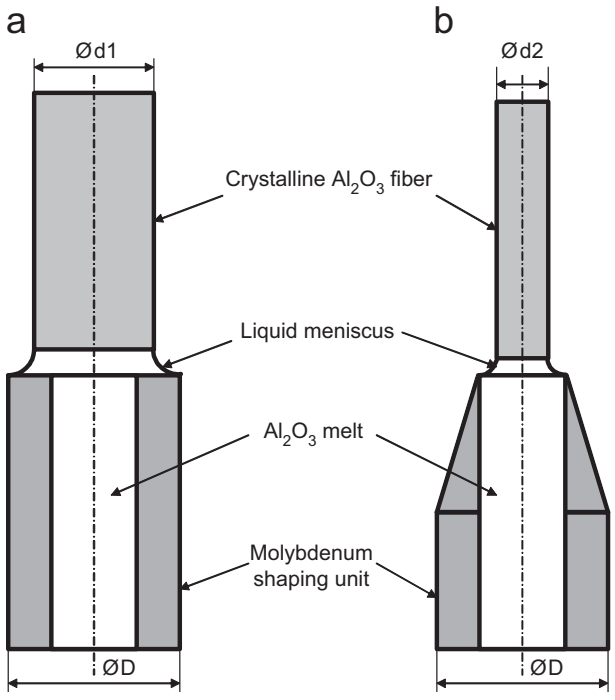

Fig. 18. Schematic diagram of two shaping units designed for pulling single crystal Al_2O_3:C fibers.

the melt. Two shaping unit designs are shown in Fig. 18. The surface tension of the aluminum oxide melt and the wetting properties of molybdenum were used to form a crystal with a diameter less than the diameter of the shaping unit, which is made of thin-walled molybdenum tubing. Thus, fibers with diameters less than 300 μm may be obtained. The design depicted in Fig. 18(b) produces fibers of smaller diameter, whereas

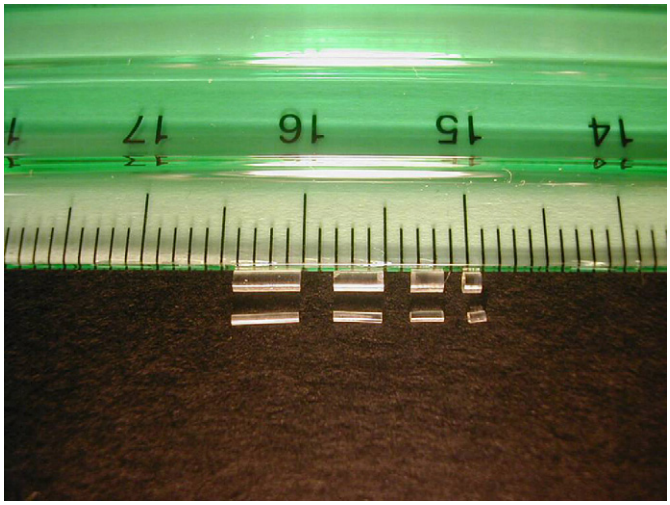

Fig. 19. Al_2O_3:C fibers for *in vivo* and *in vitro* OSL dosimetry.

shaping unit design depicted in Fig. 18(a) gives a smoother fiber surface and allows for better diameter control. Figs. 19–23 show Al_2O_3:C fibers at a different stages of production: after cutting and polishing, coupled to a silica fiberoptic guide and assembled into a fiberoptic probe with a standard FC connector. Other construction and coupling arrangements are possible.

Al_2O_3 fiber sensors for remote, real-time dosimetry applications should exhibit several important characteristics. In addition to the usual requirements of high sensitivity and linearity of dose response they should demonstrate low concentrations of shallow and deep traps. These last two requirements are especially important. As we have discussed, the existence of shallow traps slows down the readout process during periodic stimulation (see Fig. 24). A high concentration of deep traps

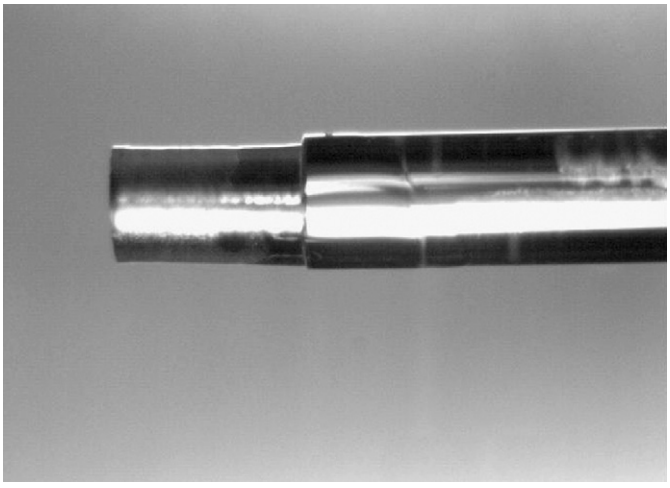

Fig. 20. Al_2O_3:C fiber attached with radiation hard optical epoxy to a silica fiberoptic guide.

Fig. 21. The assembled fiberoptic probe with Al_2O_3:C sensor.

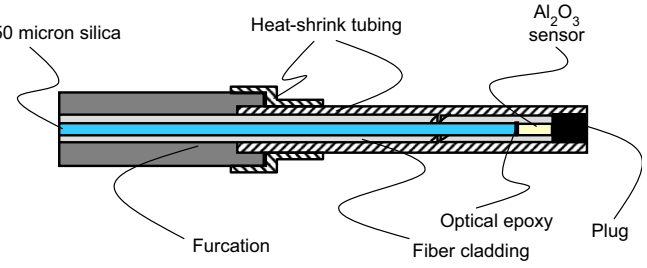

Fig. 22. The design of fiberoptic probe with Al_2O_3:C sensor.

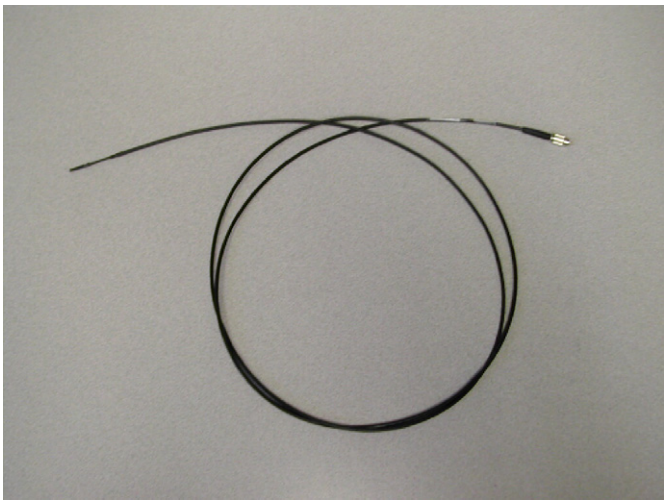

Fig. 23. The assembled fiberoptic probe with Al_2O_3:C sensor.

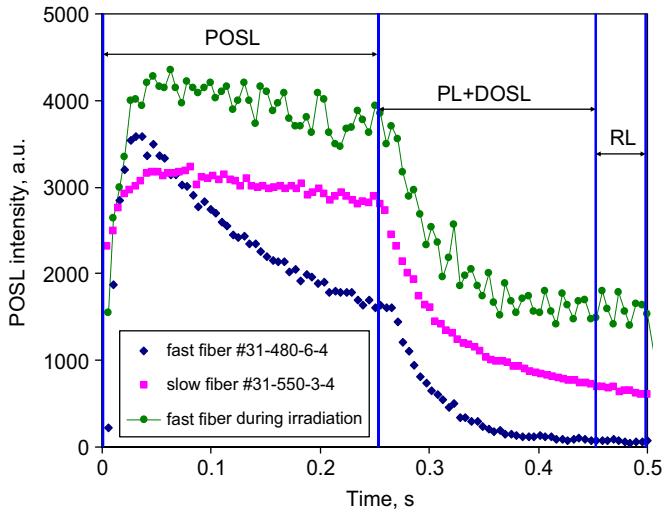

Fig. 24. OSL signal from "fast" and "slow" Al_2O_3:C fibers with periodic laser stimulation: (1 and 2) after and (3) during irradiation. One cycle of operation consists of three periods: POSL (t1), DOSL (t2) and RL (t3).

makes it difficult to completely bleach the sensor after high dose irradiation and gives rise to a changing sensitivity during the readout and irradiation process. Charge accumulated on deep traps is difficult to bleach using conventional green 532 nm light stimulation and slow release of these charge carriers produces an unwanted residual background OSL signal and changing sensitivity. Even without shallow and deep traps, however, the ultimate lower limit of the speed of OSL readout is dictated by the photoionization cross-section of the dosimetric traps and, finally, by the intrinsic luminescence lifetime (35 ms) of the main luminescence centers (F-centers).

4. OSL and RL remote optical fiber dosimetry in medical applications

4.1. Real-time in vivo monitoring of doses during radiotherapy

Therapeutic radiation oncology treatments, including teletherapy and brachytherapy as well as related procedures such as the treatment of restinosis, require the delivery of highly localized doses of radiation to patient target organs. The efficacy of the radiation treatment, however, requires knowledge

of the absorbed dose at the organ of interest to better than ±5%, with a higher risk of local recurrence or a higher risk of complications resulting from incorrect exposure. Furthermore, since it is inevitable that healthy organs and tissue will also be exposed during treatment, overexposure carries with it a concomitant risk of secondary cancers. It is necessary that all possible measures be taken to reduce the toxicity effects of undesired exposure to as low as possible. This requires both the accurate calibration of radiotherapy sources and the accurate assessment of dose at critical locations on or within the body. Thus, determination of the spatial distribution of dose to tissue from the source is an essential aspect of effective health care and treatment. Similar considerations also apply to related radiodiagnostic procedures, such as X-ray fluoroscopy and mammography.

As a result of international regulations (ICRP, 2000) there is a growing demand to improve methods for *in vivo* measurements of the absorbed doses to patients. So far, patient monitoring has been performed using one of several available detector systems; radiochromic dye films, plastic scintillators, TL dosimeters, diode detectors, or MOSFET detectors. However, each of these systems has significant disadvantages for general-purpose external dosimetry. Apart from the scintillators, the readout system is not coupled directly to the detectors, and this in turn requires a separate post-irradiation evaluation of the dosimeters. The result is that no real-time dose or dose rate information is provided.

Ideally, a real-time *in vivo* dosimeter is needed to measure absorbed doses during exposure, mainly to provide feedback of important information to the physician during treatment. OSL is an obvious method for real-time *in vivo* measurements of absorbed doses because the stimulation of a dosimeter can be made simultaneously with the detection of luminescence via light fibers using remotely placed light sources. Since the stimulation wavelength is different from that of the emitted luminescence, CW-OSL measurements can be carried out using only a single optical fiber in connection with a suitable detection filter placed in front of a photomultiplier tube cathode. Furthermore, in addition to absorbed dose information as provided by OSL, the prompt RL signal generated by the therapy radiation source directly reflects the dose rate at any time during the treatment. Thus, in addition to a small-size sensor, the main advantages of an optical fiber dosimeter over the currently available radiation detectors used in clinical applications are the capabilities of measuring both real-time dose rate and absorbed dose. When the sensor size is similar to the field size, the sensor will provide information on the average dose distribution, rather than the dose at the center of the radiation field.

4.2. The measurement of RL

RL (the term *scintillation* is also widely used) is the prompt luminescence emitted from insulators during exposure to ionising radiation and is used for investigating radiation-induced defects and luminescence emission mechanisms in wide band-gap materials (e.g. Alonso et al., 1983; Hohenau, 1985). The phenomenon arises due to ionization of the lattice under excitation from X- or gamma sources or high-energy particles, and subsequent prompt recombination of electrons and holes, either directly across the band-gap, via excitons or via charge trapped at defect sites. TL and OSL dosimetry using wide band-gap insulators is based on the trapping of charges at deep lying defect centers during irradiation; these charges accumulate with increasing irradiation dose and are ideally time-stable. Thus, the TL/OSL defects will act competitively with free electrons and holes generated during irradiation, which would otherwise recombine to produce RL. As a result the intensity of RL may depend on the accumulated dose, and can change as competition with the TL/OSL traps changes (see Section 2, and especially Figs. 9 and 10).

Some complications of using RL as the measured signal need to be mentioned. Firstly, RL also originates in the fiber cable connected to the dosimeter. Often, the RL efficiency of the fiber material is considerably less than that of the dosimeter material such that for equal amounts of dosimeter and fiber the RL signal from the dosimeter dominates. However, the fiber is generally several meters long and there is the possibility that a considerable portion of this fiber will be exposed to the radiation field. Thus, the RL signal from the fiber is not to be ignored. A second effect relates to the Čerenkov signal that emerges from the dosimeter and the fiber when exposed to high-energy radiation. Because of the length of the fiber compared to the size of the dosimeter, the Čerenkov signal from the fiber dominates. This signal has a different physical origin from RL but cannot be distinguished from it in many cases. The net result is that a significant signal emerges from the fiber, as an unwanted background to the RL signal from the dosimeter. This effect is known as the "stem effect". In irradiation procedures such as intensity modulated radiation therapy (IMRT) in which the length of fiber exposed to the field, and the angle with respect to the radiation beam direction, both change with each exposure fragment, then the extent of the "stem effect" will also vary. An additional disadvantage of the "stem effect" is that it carries with it no spatial information in that it originates in the whole length of exposed fiber and not from the small dosimeter. Thus, if it is not separated from the dosimeter RL signal all spatial information is lost, and spatial resolution is compromised. To separate out the "stem effect" an identical fiber, but without a dosimeter attached, can be placed alongside the fiber with the dosimeter and, by assuming that the "stem effect" is the same in both fibers, the dosimeter RL signal can be obtained by subtraction (Fluehs et al., 1996).

4.3. Optical fiber dosimeters

Roy et al. (1997) designed a remote OSL dosimeter system based on rare earth doped alkaline earth sulphides (e.g. MgS) as the dosimeter material coupled to the end of an optical fiber and stimulated with an infra-red laser diode. This dosimeter system yielded a dose response from 40 μGy to 10 Gy. Justus et al. (1999a,b) developed Cu^{+}-doped quartz rods, which they used as remote fiber OSL dosimeters under stimulation with

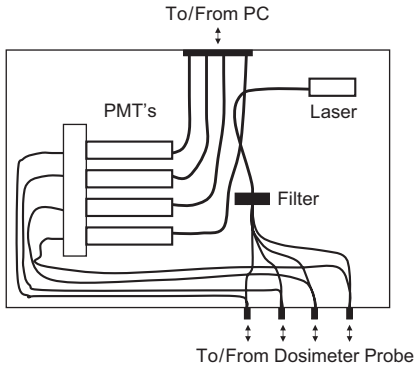

Fig. 25. Schematic diagram of a remote multiple optical fiber dosimeter system (from Huston et al., 2001).

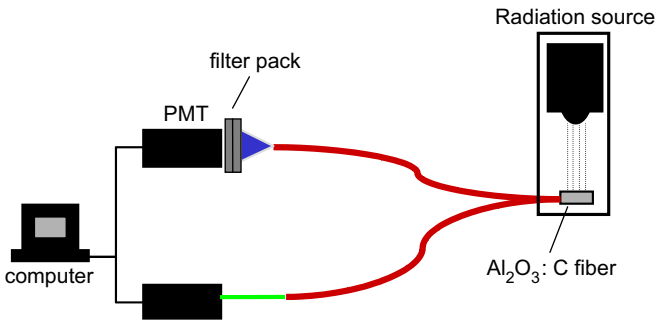

Fig. 26. Schematic of a dual-fiber real-time test arrangement using an Al_2O_3:C fiber dosimeter (from Polf et al., 2002).

790 nm light from a GaAs laser. The OSL characteristics of Cu^+-doped quartz is significantly different from that of natural quartz which makes it possible to use low-energy light for stimulation. Huston et al. (2001) constructed fiber dosimeters by drawing a 20 mm diameter by 1 m long Cu^+-doped glass rod into a 1 km length of 400 μm diameter. This fiber was used to construct a four-channel fiberoptic dosimeter system for monitoring the dose delivered to patients undergoing cancer radiotherapy. The radiation-sensitive portion of the optical fiber dosimeter consists of a 1 mm long, 0.4 mm diameter piece of Cu-doped glass that is fusion spliced to one end of a 1 m long, 0.4 mm diameter optical fiber. A black Teflon jacket surrounds most of the fiber assembly to prevent external light from entering the fiber. The end of the fiber is coated with aluminum to reflect both the stimulation and the signal light to improve the efficiency of the dosimeter. The system, which is shown in Fig. 25, has been tested successfully over a range of 10 mGy to 10 Gy.

Ranchoux et al. (2002) reported a fiber-based remote OSL system based on Al_2O_3:C single crystals, Cu^+-doped silicate fibers and alkaline-earth sulfide (MgS). A titanium–sapphire tuneable laser was used to stimulate the Cu^+-doped silicate fiber (860 nm) and MgS (980 nm), whereas the Al_2O_3:C was stimulated using 514.5 nm light from an argon laser. Polf et al. (2002) examined Al_2O_3:C optical fibers for their potential use as real-time luminescence dosimeters for use in radiotherapy. The OSL and RL responses of the Al_2O_3:C fiber probes were measured and it was found that the RL and OSL signals increased linearly with dose rate and the absorbed dose, respectively, within the dose range actual in radiotherapy (0.5–85 Gy). Polf et al. (2002) designed a dual-fiber system using the green light from a 40 mW Nd:YAG laser to stimulate the OSL signal. RL was experimentally generated using a 100 mCi $^{90}Sr/^{90}Y$ source. The OSL response as a function of dose was linear in the dose range 50 mGy to 10 Gy and the OSL signal increased for doses up to 100 Gy. Fig. 26 shows a schematic diagram of the dual-fiber system. Fig. 27 shows the OSL response as a function of absorbed dose. Fig. 27a compares the real-time OSL (RT/OSL) signal with the standard OSL signal from the same fiber. The latter has been obtained by irradiating to the doses indicated and reading the corresponding OSL. Fig. 27b shows

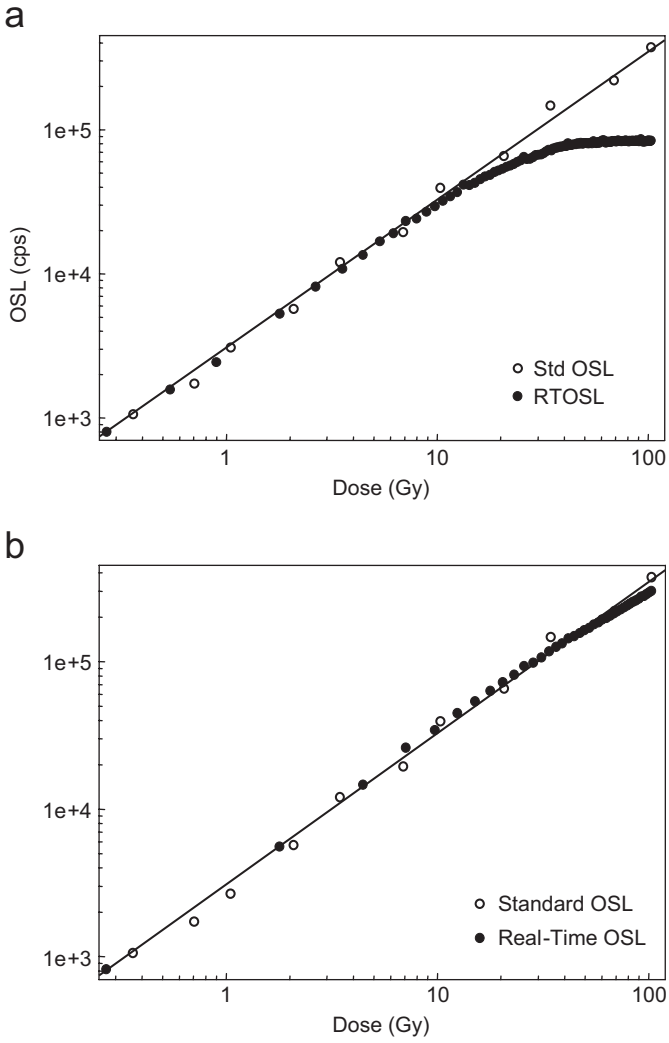

Fig. 27. OSL as a function of dose measured using the dual-fiber dosimeter. See text for explanation (from Polf et al., 2002).

the same data but with the real-time signal corrected for depletion during the real-time measurement. The under-correction at higher doses is due to a dose-dependent increase in the OSL depletion rate over this range.

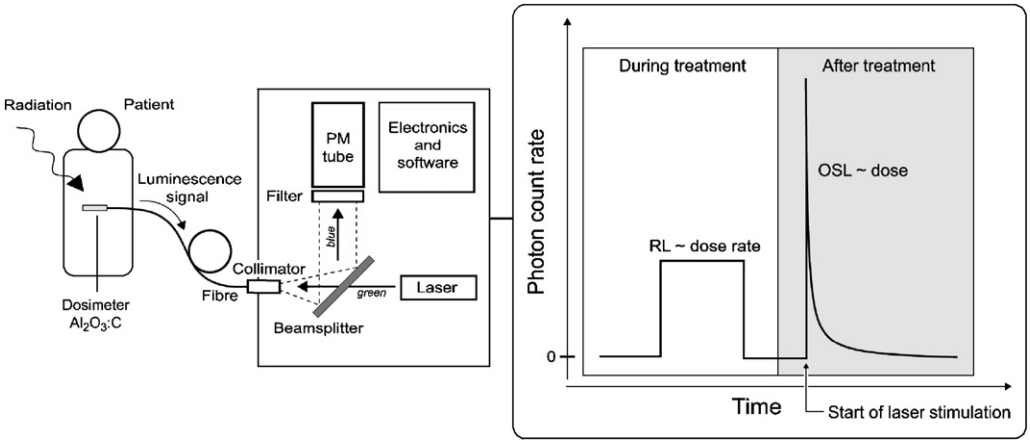

Fig. 28. Schematic diagram of a single-fiber dosimeter system. See text for explanation (from Andersen et al., 2002).

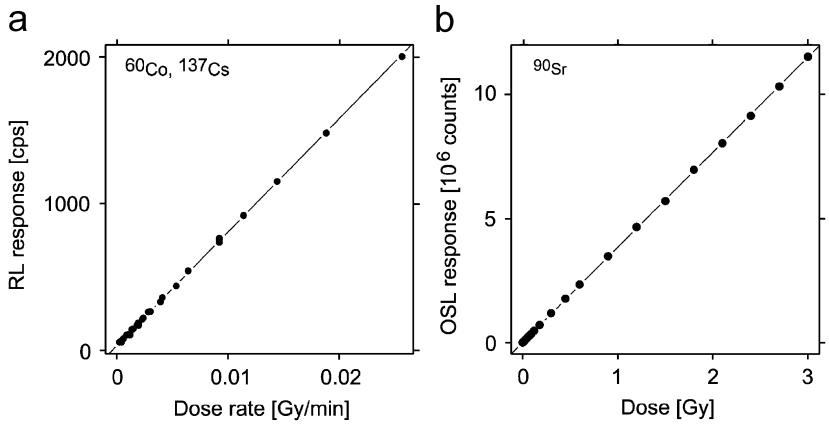

Fig. 29. RL versus beta dose rate (a) and OSL versus gamma dose (b) for the single optical fiber system (from Andersen et al., 2002).

Aznar et al. (2002) and Andersen et al. (2002) used a single-fiber system combined with a 20 mW Nd:YAG (532 nm) laser as a remote optical fiber dosimetry system for radiotherapy (see Fig. 28). To produce OSL, the laser beam is focused through a wavelength-discriminating beam-splitter positioned at 45° relative to the incident beam, and via the light fiber into the dosimeter. The OSL is transmitted from the dosimeter in the same fiber and reflected through 90° onto the photocathode of a miniature PM tube. A narrow UV band transmission filter (e.g. Hoya U-340) mounted in front of the photocathode rejects the scattered green light from the laser. Figs. 29a and b show the RL response versus ^{137}Cs gamma dose rate and the OSL response versus ^{90}Sr/^{90}Y beta dose, respectively, obtained with the one-fiber system. Fig. 30 shows that a reproducibility of less than 0.5% could be obtained when exposing the Al_2O_3:C fiber to clinical beams of 6 and 18 MV photons, and 20 MV electrons. Also Gaza et al. (2004) recently described single-fiber RL/OSL Al_2O_3:C dosimeter systems for recording real-time dose rates and absorbed doses in radiotherapy. Single-crystals of Al_2O_3:C, with typical diameters of the order of 500 μm, as described above, were used.

A typical single-fiber RL/OSL reader is shown in Fig. 31. Green light (532 nm) from a Nd:YAG laser is fed into the optical fiber and stimulates OSL from the dosimeter connected at the distal end. The blue luminescence signal (~ 420 nm) from the sample is collected through the same optical fiber, reflected through 90° by a dichroic beam splitter and fed to the light detector (PMT). A filter pack placed in front of the PMT separates the blue OSL signal from the green background of scattered laser light. A TTL signal modulating the stimulation light output can be applied either directly to the laser or via an opto-mechanical shutter. All components described above are packed in light-tight boxes, and full automatic operation of the reader is achieved by controlling them externally by a PC computer equipped with a DAQ-card and running a dedicated software. Continuous-wave (CW) lasers used typically have optical output powers ranging from 20 to 100 mW. Similar systems have been demonstrated utilizing 50 mW pulsed lasers. The width of the laser pulses was approximately 20 ns, at a repetition frequency of 4 kHz (Gaza et al., 2004).

4.4. Measurement procedures and data processing algorithms

Two fundamental approaches for measuring the luminescence signals and corresponding algorithms for dose and dose

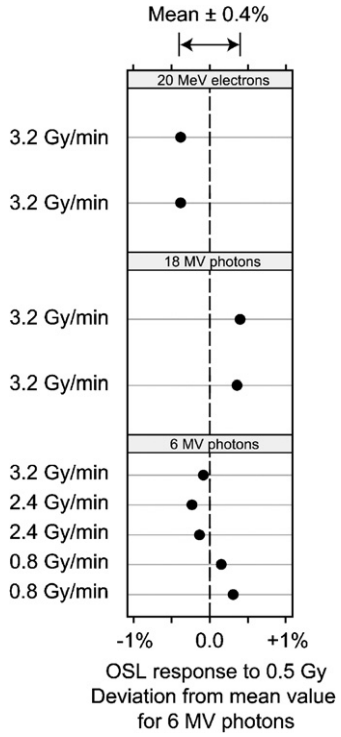

Fig. 30. Reproducibility measurements using the single optical fiber system in clinical beams. The OSL response is normalized to that obtained using 6 MV photons. As seen, the precision is $< 0.5\%$ (from Andersen et al., 2002).

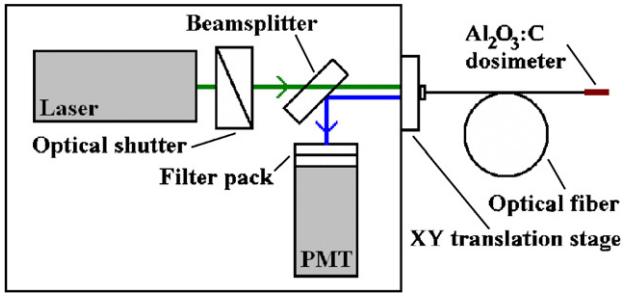

Fig. 31. Diagram of an RL/OSL single-fiber reader (from Gaza et al., 2004).

rate calculations from the raw data can be described (Gaza et al., 2004).

4.4.1. RL and post-irradiation OSL

The first part of this measurement procedure (Fig. 32) serves to measure the RL signal emitted during treatment irradiation from an initially bleached sample, in the absence of laser light stimulation. The dose rate is obtained in real time from the measured RL intensity using a mathematical algorithm at rates of 10–100 readings/s. In agreement with reports from other sources (Erfurt et al., 2000), the RL sensitivity of the dosimeter is found to increase with the absorbed dose according to a functional relation independent of other irradiation parameters (i.e. dose rate). With the known initial sensitivity of the bleached sample, and with the pre-calibrated dose dependence of the sensitivity, the estimation of the accumulated absorbed dose and

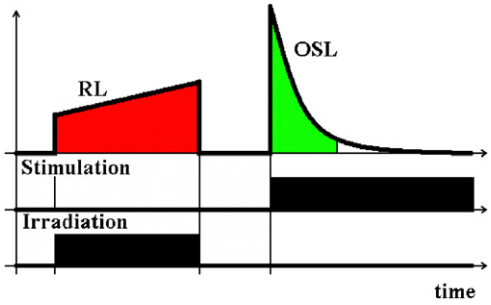

Fig. 32. The RL and post-irradiation OSL measurement procedure (from Gaza et al., 2004).

dose rate is performed in parallel with an iterative sensitivity correction.

During the second part of the measurement, after the irradiation has ended, the stimulation laser is turned on and the optically stimulated signal, with the usual decaying shape, is recorded. The OSL for a given amount of stimulation is proportional to the dose absorbed in the dosimeter during irradiation. The post-irradiation measurement will not be affected by the so-called "stem effect" (noted above).

As outlined in Fig. 32, the RL-signals from Al_2O_3:C optical dosimeter probes increase with time even though the dose rate is constant. For example, a beam of 6 MV photons gives an RL-signal that increases about 1.3% per second for a dose rate of 3.2 Gy/min. One potential solution to this "slope problem" has been addressed by Gaza et al. (2004). A simple computational algorithm was used to correct the raw RL-signal for sensitivity changes during the irradiation such that an accurate real-time estimate of the dose rate can be made. An important feature of such an approach is that it leaves the OSL-signal unaffected for subsequent estimation of the accumulated dose.

The tested algorithm is based on the assumption that the RL-sensitivity (i.e. the RL-signal per dose-rate unit) is a function only of the dose received by the probe since it was last bleached. Furthermore, it assumes that sensitivity changes can be fully characterized in a single calibration experiment. Measurements are conducted at a relatively fast rate (e.g. with 10 or 100 readings/s) and so the accumulated dose during the first reading is small, such that the RL-sensitivity can be safely set to the value read from the calibration curve at zero dose. This value and the raw RL-signal are used to compute the dose during that reading and this is added to the total dose. The initial sensitivity estimate from this may be revised (i.e. an iterative solution may be applied to get consistency between dose and sensitivity changes). During subsequent readings it is possible to keep track of the total dose and correct the RL-sensitivity accordingly.

Benchmark tests have been carried out using an X-ray irradiation facility (Andersen et al., 2002). The advantage of using an X-ray system is that the dose-rate is proportional with tube current such that well-controlled irradiations can be produced, for example using linearly increasing or decreasing (ramped) dose rates. Fig. 33 shows that the estimated real-time dose rate in one benchmark test is in good agreement with the reference

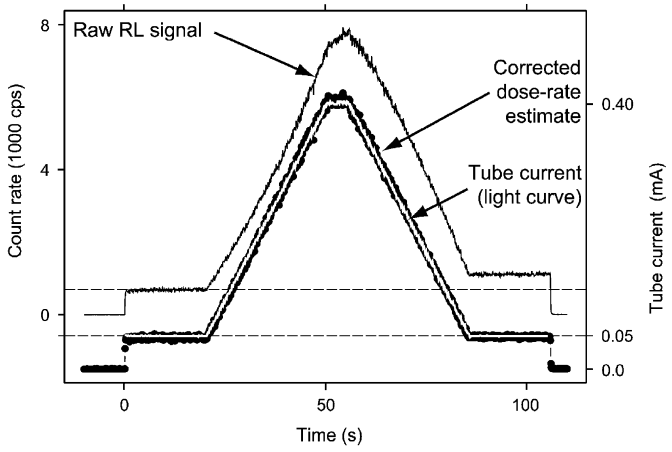

Fig. 33. Dose rate of X-rays estimated using the RL measurements and the RL algorithm. See text for explanation (from Gaza et al., 2004).

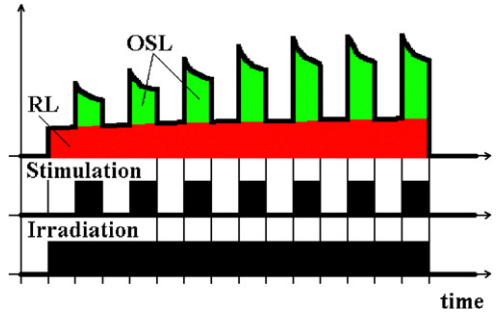

Fig. 34. The periodic OSL stimulation procedure (from Gaza et al., 2004).

values (i.e. the controlled tube current). Another benchmark test based on a set of fixed values of the tube currents (first 10 s at 0.05 mA, then 10 s at 0.1 mA, etc.) gave similar results. The two tests were made using the same calibration curve and bleaching the probe between the tests. This investigation demonstrates that the genuine RL signal indeed may be used for real-time estimation of the dose rate. Since experiments have shown that the initial RL signal (i.e. the RL response at zero dose) is reproducible and relatively independent of beam quality (Aznar et al., 2004), it is suggested that the RL-sensitivity is a function only of the accumulated dose (and not, for example, dose rate or beam quality).

4.4.2. Periodic OSL stimulation

Periodic laser stimulation during the entire duration of irradiation is used as a temporal method of discriminating the OSL signal modulated by the optical stimulation from the background luminescence emitted by the sample and the optical fiber. As already described in Section 2, the luminescence signal from the sample measured in the absence of laser stimulation consists of the RL from the Al_2O_3:C dosimeter, and the "stem effect" from the light guide. When laser stimulation is applied, a supplemental OSL signal from the dosimeter is added to any RL and "stem effect" background (Fig. 34). The OSL signal can be isolated from the background luminescence using the procedures already outlined in Section 2.

The OSL signal is proportional to the concentration of filled traps at the time the stimulation is applied. In the 'periodic stimulation' mode, the filled trap populations are affected by two processes with opposite effects: irradiation and optical stimulation. While the trap population increases due to irradiation at a rate proportional to the absorbed dose rate, a fraction F_D of the traps will be depleted each time the laser stimulation is applied. Thus, in order to recover the proportionality between OSL and the absorbed dose, the OSL signal recorded during the nth stimulation period has to be corrected for the depletion that occurred during the $(n-1)$ previous stimulations. The nth corrected OSL signal $\mathrm{OSL}'(n)$ can then be calculated according to the formula

$$\mathrm{OSL}'(n) = \mathrm{OSL}(n) + \sum_{i=1}^{n-1} \mathrm{OSL}(i) \cdot F_D(i), \tag{22}$$

where $\mathrm{OSL}(n)$ is the intensity of the nth measured OSL, and the second term in the sum accounts for the total previous depletion. The depletion factor F_D varies during an experiment. The OSL signal consists of multiple components that originate from several traps, with different characteristic decay times. The overall shape of the decay, and therefore the value of the depletion factor F_D, is dictated by the relative magnitudes of the components in the total OSL signal. In turn, the components' intensities depend, among other factors, on the dose rate and on the history of the sample. During a periodic stimulation measurement, information regarding both the intensity and the shape of each OSL curve is recorded. F_D is estimated from the shape of the OSL curve, and is then used in Eq. (22) to calculate the corrected value $\mathrm{OSL}'(n)$. An important advantage of the periodic stimulation procedure is the lack of saturation effects in the detector. Rather, a dynamic equilibrium between the processes of trap filling during irradiation, and depletion during stimulation will occur for a sufficiently long irradiation at a fixed dose rate, and thus the detector will not saturate.

The measurement procedure and algorithm using the periodic stimulation procedure have been tested for repeatability and linearity of the dose response using an X-ray source. They were also used for testing the reproducibility of speed of reaction to a sudden transition in dose rate using a ^{90}Sr source for which absorbing filters placed in front of the source could be moved quickly, thereby causing the dose rate to change suddenly Gaza et al. (2004). Fig. 35 presents the linearity of the dose rate (calculated using the above OSL correction algorithm) with the X-ray tube current. The reproducibility of the measurements at all currents, except the smallest one, is better than 2%. Fig. 36 depicts data obtained during the ^{90}Sr irradiation. Data points were taken with a resolution of about 2 s. For each point, laser stimulation was applied for 500 μs. The irradiation dose rate was abruptly switched between two values in the range of interest for radiotherapy, 55.4 and 177 mGy/s. In spite of the slow changes in the shape of the real-time OSL, the corrected OSL using Eq. (22) follows the behavior of the dose rate.

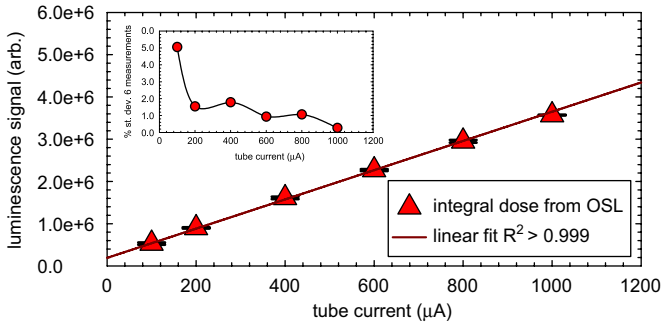

Fig. 35. Linearity of dose rate versus X-ray tube current. The dependence is obtained using the periodic OSL stimulation procedure (from Gaza et al., 2004).

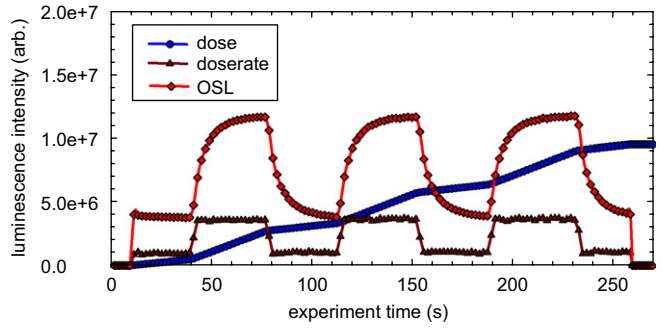

Fig. 36. The OSL signal for sudden dose rate transitions measured using the periodic OSL stimulation procedure (from Gaza et al., 2004).

4.5. Clinical applications

A variety of RL/OSL optical fiber probes has been tested using photon and soft X-ray beams at the radiotherapy facilities at Malmö University Hospital (Sweden) and photon beams at the radiotherapy facilities at the National University Hospital (Copenhagen, Denmark) (Aznar et al., 2004). When used in RL and post-irradiation OSL mode the probes generally show a linear response for both dose and dose rate over several orders of magnitude, and the reproducibility when exposed to 50 kV X-rays has been found to be 0.2% (1 SD) (Andersen et al., 2002).

4.5.1. Depth and lateral dose distributions

It is important from a clinical point-of-view to evaluate the ability of a new dosimeter to resolve depth-dose distributions and lateral profiles. RL/OSL data have been compared with those obtained using commercially available p-doped Si-diode detectors (Aznar et al., 2004). Fig. 37 shows depth-dose distributions in water obtained with 6 and 18 MV beams, respectively, using a $10 \times 10\,cm^2$ field from a Varian Clinac 2300EX set at 300 MU/min, corresponding to 3 Gy/min at the depth-dose maximum. All data have been normalized to the depth-dose maximum.

In Fig. 38, it can be observed that the largest discrepancy between diode and RL/OSL data occurs at shallow depths. This

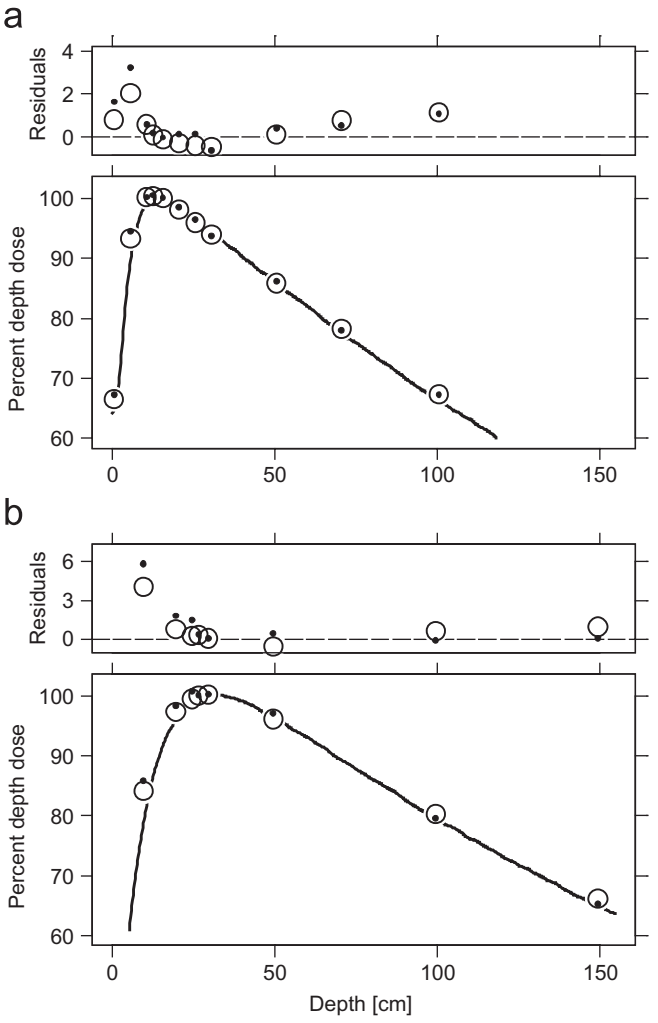

Fig. 37. Depth-dose distributions normalized to the maximum absorbed dose. OSL and RL results are plotted versus diode data (solid lines) for 6 MV (a) and 18 MV photons (b). Residual graphs show the difference between luminescence data and diode data. Hollow symbols: OSL, solid symbols: RL (from Aznar et al., 2004).

is explained partly by the positioning uncertainty in a high-dose gradient as well as by the well-known under-response of diodes at shallow depth (Heydarian et al., 1996). Beyond the build-up region, the agreement between diode and RL/OSL data is better than 1% (1SD).

These results show that the spatial resolution of the RL/OSL detector system makes it suitable for measurements of depth and lateral dose distributions in clinical photon beams.

4.5.2. In vivo measurements in radiotherapy: IMRT head and neck

The RL/OSL dosimetry system has been used to determine the dose delivered to patients during the first fraction of an IMRT head and neck treatment (Aznar et al., 2004). A catheter containing two small (ø 0.48 mm × 2 mm) RL/OSL optical fibers was inserted through the patient's nose, and positioned down the esophagus (see Fig. 38). Lead markers were positioned at the distal end of the catheter to aid the localization

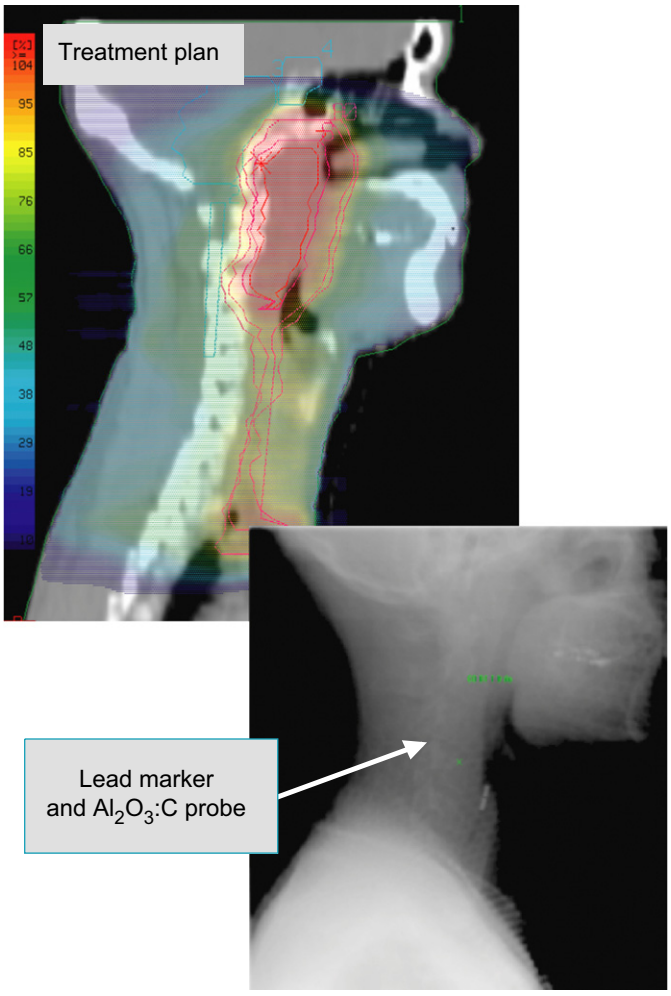

Fig. 38. Optical fiber Al_2O_3:C dosimeter used with a head and neck cancer patient in radiotherapy (from Aznar et al., 2004).

of the detector crystals. The plan was to deliver an absorbed dose of 2.00 Gy to the target volume, using a 6 MV beam of a Varian Clinac 2300EX equipped with a dynamic MLC. Calibration of the RL/OSL system was performed directly before and after the treatment by delivering four different absorbed doses to the two detectors using fixed fields and a solid water phantom. In a typical case, the absorbed dose for the patient treatment was determined to be 1.76 ± 0.05 Gy, where the indicated uncertainty is estimated from the calibration measurements and positioning relative to the point of dose evaluation in the treatment planning system (TPS). In comparison the dose delivered to the position of the detectors according to the TPS was calculated to be 1.85 Gy. The observed difference between measured dose *in vivo* and TPS is then 0.09 ± 0.05 Gy.

4.5.3. In vivo measurements in mammography

The small size OSL dosimeter probes have also been used in RL mode for real-time determinations of dose rates and doses to women's breasts during mammography examinations. Due to their small size and characteristic shape, these probes can be placed on the body surface or in the field of view during the exam, without compromising the reading of the resulting mammogram. The time resolution of such a system can be set as high as 10 ms, which means that the RL feature of the dosimeter can be used to visualize variations of the dose rate delivered by a mammography unit within one single exposure. The sensitivity of the probe is high, and doses below 100 μGy can be measured. This indicates a potential use for the measurement of both entrance and exit doses (e.g. by using two probes simultaneously). The typical reproducibility of measurements in mammography is within 3% (1 SD) for both RL and OSL data for X-ray energies ranging from 23 to 35 kV.

5. Summary and conclusions

OSL technique already became a successful tool in personal radiation dosimetry, geological and archeological dating, and in radiation diagnostic imaging. Significant advances were made recently in the theoretical study of OSL that explain the behavior of radiation sensitive materials with several types of dosimetry traps, recombination centers and competing deep traps. Progress in material, detector and instrumentation engineering allowed for new promising developments of OSL application in the medical field.

The results described in this paper show that the new RL/OSL dosimetry system has high potential to be used for *in vivo* dosimetry in both radiation therapy and diagnostic mammography. The reproducibility is suitable for *in vivo* applications and the RL/OSL probes have good features for photon radiation therapy in terms of sensitivity, dose rate dependence and energy dependence.

RL/OSL measurements have a potential interest in situations where entrance dose measurements are not desirable, such as intra-cavity treatments (e.g. prostate or gynecological sites). In these situations, RL/OSL would have practical advantages: the optical fiber system enables an on-line read-out, low doses (e.g. to radiosensitive organs) can be detected, and small probes can be used to minimize the interference with the patient treatment. At present, due to the high sensitivity of Al_2O_3:C to ionizing radiation, the crystal can be made very small without compromising the accuracy of the absorbed dose determinations: present technology can provide Al_2O_3:C with diameters as small as 300 μm, which should still have suitable sensitivity for radiotherapy applications. The energy dependence of the detector was found to be 0.6% (1 SD) for the relevant energy range in radiotherapy.

References

Akselrod, M.S., Gorelova, E.A., 1993. Deep traps in highly sensitive α-Al_2O_3:C TL crystals. Nucl. Tracks Radiat. Meas. 21, 143–146.

Akselrod, M.S., McKeever, S.W.S., 1999. A radiation dosimetry method using pulsed optically stimulated luminescence. Radiat. Prot. Dosim. 81, 167–176.

Akselrod, M.S., Kortov, V.S., Kravetsky, D.J., Gotlib, V.I., 1990. Highly sensitive thermoluminescent anion-defective α-Al_2O_3:C single crystal detectors. Radiat. Prot. Dosim. 32, 15–20.

Akselrod, M.S., Lucas, A.C., Pulf, J.C., McKeever, S.W.S., 1998a. Optically stimulated luminescence of Al_2O_3. Radiat. Meas. 29, 391–398.

Akselrod, M.S., Agersnap Larsen, N., Whitley, V., McKeever, S.W.S., 1998b. Thermal quenching of F-centre luminescence in, Al_2O_3:C. J. Appl. Phys. 84, 3364–3373.

Akselrod, M.S., Agersnap Larsen, N., McKeever, S.W.S., 2000. A procedure for the distinction between static and dynamic radiation exposures of personal radiation badges using pulsed optically stimulated luminescence. Radiat. Meas. 32, 215–225.

Alonso, P.J., Halliburton, L.E., Kohnke, E.E., Bossoli, R.B., 1983. X-ray induced luminescence in crystalline SiO_2. J. Appl. Phys. 54, 5369–5375.

Andersen, C.E., Aznar, M.C., Bøtter-Jensen, L., Back, S.A.J., Mattson, S., Medin, J., 2002. Developments of optical fiber luminescence techniques for real-time in vivo dosimetry for radiotherapy. In: Presented at the IAEA Symposium on Standards and Codes of Practice in Medical Radiation Dosimetry, Vienna, November 25–28, 2002.

Antonov-Romanovskii, V.V., Keirum-Marcus, I.F., Poroshina, M.S., Trapeznikova, Z.A., 1956. IR stimulable phosphors. In: Conference of the Academy of Sciences of the USSR on the Peaceful Uses of Atomic Energy, Moscow, 1955. USAEC Report AEC-tr-2435, pp. 239–250.

Aznar, M.C., Polf, J.C., Akselrod, M.S., Andersen, C.E., Back, S.A.J., Bøtter-Jensen, L., Mattson, S., McKeever, S.W.S., Medin, J., 2002. Real-time optical fiber dosimetry in radiotherapy. In: Presented at the American Association of Physics in Medicine (AAPM). 44th Annual Meeting in Montreal, July 14–18. Phys. Med. Biol. 29, 1371.

Aznar, M.C., Andersen, C.E., Bøtter-Jensen, L., Bäck, S.A.J., Mattsson, S., Kjær-Kristoffersen, F., Medin, J., 2004. Real-time optical fiber luminescence dosimetry for radiotherapy: physical characteristics and applications in photon beams. Phys. Med. Biol. 49 (9), 1655–1669.

Bernhardt, R., Herforth, L., 1974. Radiation dosimetry by optically stimulated phosphorescence of CaF2: Mn. In: Proceedings of Fourth International Conference on Luminescence Dosimetry.Krakow, Poland, pp. 1091–1104.

Bøtter-Jensen, L., Wintle, A.G., McKeever, S.W.S., 2003. Optically Stimulated Luminescence Dosimetry. Elsevier, Amsterdam.

Bräunlich, P., 1979. Introduction and basic principles. In: Bräunlich, P. (Ed.), Thermally Stimulated Relaxation in Solids. Springer, Berlin, pp. 1–33.

Bräunlich, P., Schafer, D., Scharmann, A., 1967. A simple model for thermoluminescence and thermally stimulated conductivity of inorganic photoconducting phosphors and experiments pertaining to infra-red stimulated luminescence. In: Proceedings of the First International Conference on Luminescence Dosimetry, Stanford, June 1965. USAEC, pp. 57–73.

Buckman, W.G., 1972. Aluminum oxide thermoluminescence properties for detecting radiation. Health Phys. 22, 402.

Colyott, L.E., Akselrod, M.S., McKeever, S.W.S., 1996. Phototransferred thermoluminescence in α-Al_2O_3. Radiat. Prot. Dosim. 65, 263–266.

Erfurt, G., Krbetschek, M.R., Trautmann, T., Stolz, W., 2000. Radioluminescence (RL) behaviour of Al_2O_3:C—potential for dosimetric applications. Radiat. Meas. 32, 735–739.

Evans, B.D., Stapelbroek, M., 1978. Optical properties of the F^+ centre in crystalline Al_2O_3. Phys. Rev. B 18, 7089–7098.

Fluehs, D., Heintz, M., Indenkampen, F., Wieczorek, C., Kolanski, H., Quast, U., 1996. Direct reading measurement of absorbed dose with plastic scintillators—the general concept and applications to ophthalmic plaque dosimetry. Med. Phys. 23, 427–434.

Gaza, R., McKeever, S.W.S., Akselrod, M.S., Akselrod, A., Underwood, T., Yoder, C., Andersen, C.E., Aznar, M.C., Marckmann, C.J., Bøtter-Jensen, L., 2004. A fiber-dosimetry method based on OSL from Al_2O_3:C for radiotherapy applications. Radiat. Meas. 38 (4–6), 809–812.

Heydarian, M., Hoban, P.W., Beddoe, A.H., 1996. A comparison of dosimetry techniques in stereotactic radiosurgery. Phys. Med. Biol. 41, 93–100.

Hohenau, W., 1985. On the kinetics of X-ray induced luminescence in natural quartz. Phys. Stat. Sol. (a) 88, 267–276.

Huntley, D.J., Godfrey-Smith, D.L., Thewalt, M.L.W., 1985. Optical dating of sediments. Nature 313, 105–107.

Huston, A.L., Justus, B.L., Falkenstein, P.L., Miller, R.W., Ing, H., Altemus, R., 2001. Remote optical fibre dosimetry. Nucl. Instrum. Methods B 184, 55–77.

International Commission on Radiological Protection, 2000. Prevention of accidental exposures to patients undergoing radiation therapy. ICRP Publication 86. Ann. ICRP 30, 1–70.

Justus, B.L., Pawlovich, K.J., Merritt, C.D., Huston, A.L., 1999a. Optically and thermally stimulated luminescence characteristics of Cu^+-doped fused quartz. Radiat. Prot. Dosim. 81, 5–10.

Justus, B.L., Merritt, C.D., Pawlovich, K.J., Huston, A.L., Rychnovsky, S., 1999b. Optically stimulated luminescence dosimetry using doped fused quartz. Radiat. Prot. Dosim. 84, 189–192.

Lapraz, D., Iacconi, P., Sayady, Y., Keller, P., Barthe, J., Portal, G., 1988. Some thermoluminescence of an α-Al_2O_3 sample. Phys. Stat. Sol. (a) 108, 783–794.

Lee, K.H., Crawford, J.H., 1977. Electron centers in single crystal Al_2O_3. Phys. Rev. B 15, 4065–4074.

McDougall, R.S., Rudin, S., 1970. Thermoluminescent dosimetry of aluminum oxide. Health Phys. 19, 281–283.

McKeever, S.W.S., 2001. Optically stimulated luminescence dosimetry. Nucl. Instrum. Methods B 184, 29–54.

McKeever, S.W.S., Moscovitch, M., 2003. On the advantages and disadvantages of optically stimulated luminescence dosimetry and thermoluminescence dosimetry. Radiat. Prot. Dosim. 104, 263–270.

McKeever, S.W.S., Moscovitch, M., Townsend, P.D., 1995. Thermoluminescence Dosimetry Materials: Properties and Uses. Nuclear Technology Publishers, Ashford.

McKeever, S.W.S., Akselrod, M.S., Markey, B.G., 1996. Pulsed optically stimulated luminescence dosimetry using α-Al_2O_3:C. Radiat. Prot. Dosim. 65, 267–272.

McKeever, S.W.S., Bøtter-Jensen, L., Agersnap Larsen, N., Duller, G.A.T., 1997. Temperature dependence of OSL decay curves: experimental and theoretical aspects. Radiat. Meas. 27, 161–170.

Mehta, S.K., Sengupta, S., 1976. Gamma dosimetry using Al_2O_3:Si,Ti thermoluminescent phosphor. Phys. Med. Biol. 21, 955–964.

Meijerink, A., Schipper, W.J., Blasse, G., 1991. Photostimulated luminescence and thermally stimulated luminescence of Y2SiO5-Ce, Sm. J. Phys. D 24, 997–1002.

Miller, S.D., Endres, G.W.R., McDonald, J.C., Swinth, K.L., 1988. Cooled optically stimulated luminescence in CaF2:Mn. Radiat. Prot. Dosim. 25, 201–205.

Molnar, G., Benabdesselam, M., Borossay, J., Iacconi, P., Lapraz, D., Akselrod, M.S., 2002. Influence of the irradiation temperature on the dosimetric and high temperature TL peaks of Al_2O_3:C. Radiat. Prot. Dosim. 100, 139–142.

Osvay, M., Biro, T., 1980. Aluminum oxide in TL dosimetry. Nucl. Instrum. Methods 175, 60–61.

Pokorny, P., Ibarra, A., 1994. On the origin of the thermoluminescence of α-Al_2O_3:Cr, Ni. J. Phys. Condens. Matter 5, 7387–7396.

Polf, J.C., McKeever, S.W.S., Akselrod, M.S., Holmstrom, S., 2002. A real-time, fiber optic dosimetry system using Al_2O_3 fibers. Radiat. Prot. Dosim. 100, 301–304.

Polf, J.C., Yukihara, E.G., Akselrod, M.S., McKeever, S.W.S., 2004. Real-time luminescence from Al_2O_3 fiber dosimeters. Radiat. Meas. 38, 227–240.

Pradhan, A.S., Ayyangar, K., 1977. Radiation dosimetry by photostimulated luminescence of CaSO4:Dy. Int. J. Appl. Radiat. Isot. 28, 534–535.

Ranchoux, G., Magne, S., Bouvet, J.P., Ferdinand, P., 2002. Fiber remote optoelectronic gamma dosimetry based on optically stimulated luminescence of Al_2O_3:C. Radiat. Prot. Dosim. 100, 255–260.

Rieke, J.K., Daniels, F., 1957. Thermoluminescence studies of aluminum oxide. J. Phys. Chem. 61, 629–633.

Roy, O., Magne, S., Gaucher, J.C., Albert, L., Dusseau, L., Bessiere, J.C., Ferdinand, P., 1997. All optical fiber sensor based on optically stimulated luminescence for radiation detection. In: Presented at the 12th International Conference on Optical Fiber Sensors OFS'97, Williamsburg, Virginia, USA, October 28–31, 1997.

Sanborn, E.N., Beard, E.L., 1967. Sulfides of strontium, calcium, and magnesium in infrared-stimulated luminescence dosimetry. In: Proceedings of First International Conference on Luminescence Dosimetry. pp. 183–191.

Schipper, W.J., Hamelink, J.J., Blasse, G., 1994. The X-ray storage properties of barium phosphate doped with trivalent rare earth ions. Phys. Stat. Sol. (a) 141, 231–238.

Sonada, M., Takano, M., Miyahara, J., Kato, H., 1983. Computed radiography utilizing scanning laser stimulated luminescence. Radiography 148, 833–837.

Stoneham, A.M., 1975. Theory of Defects in Solids. Clarendon Press, Oxford.

Tochilin, E., Goldstein, N., Miller, W.G., 1969. Beryllium oxide as a thermoluminescent dosimeter. Health Phys. 16, 1–7.

Trinkler, L.E., Trinkler, M.F., Popov, A.I., 1993. Stimulation energy of the X-ray storage material KBr:In. Phys. Stat. Sol. (b) 180, K31–K34.

Whitley, V.H., McKeever, S.W.S., 2000. Photoionization of deep centers in Al_2O_3. J. Appl. Phys. 87, 249–256.

Yoder, R.C., Salasky, M.R., 1997. A dosimetry system based on delayed optically stimulated luminescence. Health Phys. 72, S18–S19.

Yukihara, E.G., Whitley, V.H., Polf, J.C., Klein, D.M., McKeever, S.W.S., Akselrod, A.E., Akselrod, M.S., 2003. The effects of deep trap population on the thermoluminescence of Al_2O_3:C. Radiat. Meas. 37, 627–638.

Yukihara, E.G., Gaza, R., McKeever, S.W.S., Soares, C.G., 2004a. Optically stimulated luminescence and thermoluminescence efficiencies for high-energy heavy charged particle irradiation in Al_2O_3:C. Rad. Meas. 38, 59–70.

Yukihara, E.G., Whitley, V.H., McKeever, S.W.S., Akselrod, A.E., Akselrod, M.S., 2004b. Effect of high-dose irradiation on the optically stimulated luminescence of Al_2O_3:C. Radiat. Meas. 38, 317–330.